Biochimica et Biophysica Acta 1838 (2014) 2882–2898

Contents lists available at ScienceDirect

Biochimica et Biophysica Acta

journal homepage: www.elsevier.com/locate/bbamem

Translocation mechanism of P-glycoprotein and conformational changes occurring at drug-binding site: Insights from multi-targeted molecular dynamics

Rameshwar Prajapati, Abhay T. Sangamwar *

Department of Pharmacoinformatics, National Institute of Pharmaceutical Education and Research (NIPER), Sector-67, S. A. S. Nagar, Punjab, India

ARTICLE INFO

Article history:
Received 13 February 2014
Received in revised form 3 July 2014
Accepted 8 July 2014
Available online 25 July 2014

Keywords:
P-glycoprotein
Multi-targeted molecular dynamics
Translocation mechanism

ABSTRACT

P-glycoprotein (P-gp) is well known for multidrug resistance in drug therapy. Its over-expression results into the increased efflux of therapeutic agents rendering them inefficacious. A clear understanding of P-gp efflux mechanism and substrate/inhibitor interactions during the course of efflux cycle will be crucial for designing effective P-gp inhibitors, and therapeutic agents that are non-substrate to P-gp. In the present work, we have modeled P-gp in three different catalytic states. These models were utilized for elucidation of P-gp translocation mechanism using multi-targeted molecular dynamics (MTMD). The gradual changes occurring in P-gp structure from inward open to outward open conformation were sampled out. A detailed investigation of conformational changes occurring in trans-membrane domains (TMDs) during the course of catalytic cycle was carried out. Movements of each TM helices in response to pronounced twisting and translatory motion of NBDs were measured quantitatively. The role of intracellular coupling helices (ICHs) during the structural transition of P-gp was studied, and observed as vital links for structural transition. A close observation of displacements and conformational changes in the residues lining drug-binding pocket was also carried out. Further, we have analyzed the molecular interactions of P-gp substrates/inhibitors during the P-gp translocation to find out how stable binding interactions of a compound at drug-binding site(s) in open conformation, becomes highly destabilized in closed conformation. The study revealed striking differences between the molecular interactions of substrate and inhibitor; inhibitors showed a tendency to maintain stable binding interactions during the catalytic transition cycle.

1. Introduction

In 1976, Ling and Juliano introduced a permeability glycoprotein (P-glycoprotein, P-gp) that efficiently "pump" substrates out of tumor cells through an ATP-dependent mechanism in an unidirectional fashion [1]. P-gp is a member of ATP-binding cassette (ATP) transporter proteins, also known as ABCB1 or MDR1. It is expressed at cellular level and function as xenobiotic monitor protecting cells from toxicants [2]. Over-expression of P-gp is associated with increased efflux of therapeutic agents from their site of action. Thus, its over-expression has resulted in the reduced efficacy of many therapeutic agents like anticancer agents, antiviral agents, calcium channel blockers, neuroleptics, antiarrythmics, antimalarials and antifungals [3]. Moreover, substrate promiscuity confers this protein an abnormal ability to efflux out chemically unrelated drugs. P-gp effluxes out substrates ranging from approximately 300 to 4000 Da in mass, for instance mitomycin (334 Da), amisulpride (362 Da), flupheanzine (437 Da), daunorubicin (527 Da), docetaxel (807 Da), rapamycine (914 Da), and cyclosporine (1202 Da) [4–6].

P-gp has 1280 amino acid residues, constituting a molecular mass of approximately 170 kDa. Structurally, P-gp is a single polypeptide comprising of two homologous halves; each consisting of a trans-membrane domain (TMD) and a nucleotide binding domain (NBD). The two homologous parts are separated by an intracellular linker region of about 60 amino acid residues. Each TMD consists of six membrane spanning helices arranged in a specific pattern. Both TMDs are arranged together to form a large highly hydrophobic cavity that could accommodate multiple substrates. The NBDs are highly conserved regions, and are sites of ATP binding/hydrolysis [7–9].

P-gp has been crystallized in different catalytic forms from different organisms, but the crystal structure of human P-gp is not yet available. Recently, human mitochondrial P-gp crystal structure has been published in complex with nucleotide analogs [PDB IDs: 4AYT (rod form A), 4AYX (rod form B), 4AYW (plate form)], and in a ligand-free apo form [PDB ID: 3ZDQ] [10]. The bacterial P-gp crystal structures with relatively good resolution reported prior to 2007 were Sav1866 (*Staphylococcus aureus* transporter) and MsbA [11,12]. These bacterial

* Corresponding author at: Department of Pharmacoinformatics, National Institute of Pharmaceutical Education and Research (NIPER) S.A.S. Nagar, Punjab 160 062, India. Tel.: +91 172 2214682.
E-mail address: abhays@niper.ac.in (A.T. Sangamwar).

http://dx.doi.org/10.1016/j.bbamem.2014.07.018
0005-2736/

crystal structure templates were widely used for homology modeling of human P-gp. MsbA crystallographic structure was used to model human P-gp in open conformation (drug-binding cavity open to intracellular space, NBDs far apart). Sav1866 crystallographic structure was utilized to model closed conformation (drug-binding cavity open to extracellular space, NBDs in close proximity). The three murine P-gp crystallographic structures [13] (PDB IDs: 3G5U, 3G60 and 3G61) published by Aller et al. in 2009, were promising templates for modeling human P-gp in open conformation. However, in a recently published *Caenorhabditis elegans* P-gp crystal structure [14], Jin et al. have pointed out significant register errors in TM3, TM4 and TM5 regions in the murine P-gp crystallographic structure (corrected structure has been recently published [15]). Corrections in these errors are relevant to the identification of drug-interacting amino acids and an accurate definition of the NBD–TMD interface. Thus, the model built from murine P-gp is not much reliable for substrate binding studies. However, the crystallographic structure of *C. elegans* P-gp, with a resolution of 3.4 Å, shares less sequence identity (49%) to human P-gp as compared to that of murine P-gp (87%), but the similarities between their amino acid sequences and functional properties suggest that the structure of *C. elegans* P-gp is a reasonable starting point for substrate binding studies and mechanistic understanding of human P-gp [14].

Molecular dynamics studies have been predominantly used for elucidation of translocation mechanism and substrate binding of P-gp. Detailed depictions of ATP hydrolysis mechanisms and conformational changes taking place in response to hydrolysis were reported from MD studies on isolated NBDs [16–26]. Furthermore, full-length ABC transporter molecular dynamics simulations [27–36] gave insights into the conformational changes in TMDs and substrate binding site during substrate translocation. Recently, using MD studies researchers have reported the effect of surrounding environment on the structure and function of P-gp [37] and importance of linker region in the stability of P-gp structure [38]. However, in most of these studies murine crystallographic structure was used as template for human P-gp model building, which raises some dubiety of these studies regarding register error in murine P-gp structure.

In the present study, we have employed multi-targeted molecular dynamics (MTMD) technique to trace out catalytic transition cycle of P-gp efflux pump. The technique employs addition of an extra term to the energy function based on the mass-weighted root mean square deviation of a set of atoms in the current structure compared to the reference structure. Using MTMD, multiple reference structures can be specified through which the specified structure will move. The present structure is fitted to the target structure by the application of a force vector calculated to decrease the RMSD between the two structures.

Human P-gp was modeled in three different catalytic states; inward open (IO) (NBDs far apart), intermediate open (IIO) and outward open (OO) (NBDs in close proximity). Inward open catalytic structure of human P-gp was taken from our previously reported model developed using *C. elegans* P-gp crystal structure as a template [39]. The other two catalytic states; intermediate inward open and outward open were modeled using human mitochondrial P-gp and Sav1866 P-gp crystal structures as templates, respectively. The three catalytic structures were subjected to MTMD simulation to gain valuable insights into the P-gp efflux mechanism. In-depth analysis of shifts in TMDs was carried out during the course of catalytic cycle. Quantitative measurement of movement of NBDs and ICHs was performed. The stretching of TMs in correspondence with movement of intracellular coupling helices (ICHs) was also noticed. A detailed analysis of conformational changes occurring at drug-binding site and, the relative changes in distance and angles of drug-binding residues was carried out. A relation between the conserved apical interactions and the twisting movement of NBDs was noticed. Hydrophobic substrate gates were also observed during MTMD simulations. Furthermore, MTMD simulations were carried out with known substrates and inhibitors of P-gp to find out the relative difference in their binding pattern and the motion path they follows when efflux out by P-gp. A clear difference was noticed between substrates and inhibitors interactions during the course of P-gp structural transition. Most of the results well correlated with large body of reported biochemical and biophysical data giving substantial clues to hypothesize P-gp efflux mechanism.

2. Methods

2.1. Homology modeling

Human P-gp homology model in IO catalytic state was utilized from our previous study. *C. elegans* P-gp crystallographic structure was taken as a template to model IO catalytic state. Human mitochondrial P-gp (PDB ID: 4AYT) and Sav1866 P-gp crystal structures were used to model IIO catalytic state and OO catalytic state of human P-gp, respectively. The amino acid sequences of human P-gp, human mitochondrial P-gp and Sav1866 P-gp were retrieved from UniProtKB/TrEMBL database, primary accession numbers P08183, Q9NRK6 and Q99T13, respectively. Sequence alignment was performed on ClustalW (Figs. S1 and S2), using a gap penalty of 10 and a gap extension penalty of 0.05. Subsequently, homology modeling of human P-gp was performed on MODELLER 9v8. The linker region was not modeled. The initially generated models were evaluated by Ramachandran plot and Errat plot using PROCHECK program in SAVES server. The iterative loop refinement and energy minimization were performed to refine the obtained homology model.

2.2. Induced fit docking

2.2.1. Preparation of model and ligands for the IFD protocol

The 3D structures of the P-gp substrates and inhibitors were built on Sybyl7.1 software package. All 3D structures were minimized by Powell method. The minimization was terminated when the energy gradient convergence criteria of 0.05 kcal/mol * Å was reached or 2000 steps of minimization cycle were exceeded. Table S1 shows the list of substrates and inhibitors used in docking experiments.

Protein preparation wizard of Schrödinger suite 9.0.211 was used for structural preparations of P-gp homology model. The protein preparation includes the addition of hydrogen atoms, optimization of hydrogen bonding networks, and minimization of protein to RMSD 0.30 Å, using Optimized Potential for Liquid Simulations (OPLS) 2005 force field. The selected ligands were prepared in LigPrep and minimized using OPLS 2005 force field.

2.2.2. Induced-fit docking protocol

The IFD protocol as mentioned in IFD manual of Schrödinger 9.0.211, was followed. [40,41] In brief, Schrödinger suite uses two modules, Glide and Prime to perform IFD. The ligand flexibility and the receptor flexibility are accounted by Glide and Prime, respectively. IFD was performed in following steps. (i) The receptor was minimized applying constrain (Glide protein preparation, refinement only) with an RMSD cutoff of 0.18 Å. (ii) A softened potential (van der Waals radii scaling) was used for initial Glide docking of each ligand. Twenty poses per ligand that had a Coulomb–vdW score less than 100 and an H-bond score less than 0.05 were retained. (iii) Each protein–ligand complex was subjected to one round of Prime side chain prediction. In our study, residues of active site(s) were defined instead of considering residues within the cutoff distance from the ligand. (iv) The same set of residues and the ligand for each protein–ligand complex poses were minimized by Prime. Each pose of receptor structure reflected an induced fit to the ligand structure and conformation. (v) The protein–ligand complexes within a specified energy of the lowest-energy structure (default 30 kcal/mol) were subjected to Glide re-docking. The ligand was then rigorously docked, using default Glide settings,

into the induced-fit receptor structure.(vi) Estimation of the binding energy (IFD Score) for each output pose.

Residues reported in experimental studies [42–45] that have been implicated in drug binding were specified for active site grid generation (listed in supplementary information, Table S2). The ligand docking calculations were done on the standard precision mode of Glide software.

2.3. Molecular dynamics simulations

The generated homology models were embedded into POPC lipid bilayer. CHARMM-GUI Lipid Builder was used to embed protein structures into lipid bilayer. The coordinates of lipid bilayer were taken from OPM database. The lipid–protein systems were solvated using TIP3P water model and neutralized by the addition of counter ions. The CHARMM-GUI generated PDB files were reformatted to files that conform to the Lipid11 force field naming convention using *charmmlipid2amber.x* script. AMBER99SB force field was used for the parameterization of protein and Lipid 11 force field was used for the parameterization of POPC lipid. The final system of each membrane embedded homology model contained 340 lipid molecules, 44,313 solvent molecules, Mg^{2+} ion, ATP, ADP, Pi, 14 Na^{+} and 26 Cl^{-} ions, constituting 1,96,939 total number of atoms (Figs. S3).

Minimization of the protein–lipid systems was carried out in two successive steps. Firstly, the protein was restrained with a force constant of 50 kcal/mol/Å^2, and only solvent and lipid phase were minimized with 500 cycles of each steepest descent and conjugate gradient methods. In the second step, whole system was minimized with 500 cycles of both steepest descent and conjugate gradient. The systems were gradually heated to 310 K on NVT ensemble for 50 ps, where the protein was restrained with a force constant of 20 kcal/mol/Å^2. Equilibration was performed on NPT ensemble at 310 K temperature and 1 atm pressure for 50 ns with a restraint force constant of 20 kcal/mol/Å^2 on the protein. For entire simulation the step size was kept 2 fs. During the MD run all bonds containing hydrogen atoms were constrained using SHAKE algorithm. Langevin thermostat and barostat were used for temperature and pressure coupling. The non-bonded cutoff was kept at 8 Å, and long-range electrostatic interactions were treated by the Particle–Mesh Ewald (PME) method.

2.4. Multi-targeted molecular dynamics simulations

All MTMD simulations were carried out on AMBER 12. The equilibrated protein–lipid systems were subjected to MTMD simulations. The IO catalytic transition state was taken as initial structure and, IIO and OO catalytic states of P-gp were taken as reference structures. The root mean square deviation between IO and IIO was 8.69 Å and that between IO and OO was 12.46 Å. The IO was first targeted to IIO and then to OO transition state to trace out the catalytic cycle. The present structure was fitted to the target structure by the application of a force vector calculated to decrease the RMSD between two structures. An additional term to the energy function based on the mass-weighted root mean square deviation of a set of atoms in the current structure compared to a reference structure is added by the MTMD simulation package of AMBER 12.

Prior to MTMD simulations of protein–ligand systems, the ligand from best docked pose of each protein was extracted. The atomic charges for ligands were derived with AM1-BBC method implemented in Antechamber program of AmberTools. General amber force field (GAFF) was used to generate missing parameters of ligands using Parmchk module of Antechamber. The protein–ligand system was then embedded into POPC lipid bilayer and subjected to molecular dynamics simulation, following the similar protocol mentioned above to get an equilibrated structure for MTMD simulation. The simulation studies consisted of total 17 systems (16 with ligand and one initial without ligand). Each system was subjected to 50 ns of equilibration and 50 ns of MTMD simulation. Ptraj module of Amber tools, VMD, Pymol and xmgrace were used for trajectory analysis.

3. Results and discussion

3.1. Models of catalytic transition structures

P-gp efflux pump undergoes a large body of structural transformation from fully open inward (NBDs are far apart) to fully open outward (NBDs in close proximity) conformation state. The crystal structure of P-gp is available in different catalytic forms. In this study, we have modeled human P-gp in three different catalytic states utilizing crystallographic structural templates of *C. elegans* P-gp, human mitochondrial P-gp and Sav1866 P-gp. Though, both *C. elegans* P-gp and human mitochondrial P-gp crystal structures (PDB ID: 4AYT) are in inward open conformation, the distances between their NBDs with respect to C-α atom of conserved glutamate residues (E556 and E1201) are 39.5 Å and 26.5 Å, respectively. The respective distance in Sav1866 P-gp is 14.3 Å. Thus, mitochondrial P-gp could be utilized as an intermediate structure between inward open and outward open state for studying the catalytic transformation of P-gp. Moreover, the model generated from *C. elegans* P-gp was used as starting structure because it showed maximum consistency with reported biochemical and biophysical data [42–59] (discussed in detail further in text).

The model of human P-gp in inward open state built using *C. elegans* P-gp as template was taken from our previously reported model [39]. The models of human P-gp in intermediate inward open state and outward open state were generated using mitochondrial P-gp and Sav1866 P-gp as templates, respectively. The sequence identity of human P-gp with mitochondrial P-gp is 41% and that with Sav1866 is 17%. Sequence alignment was performed on ClustalW (Figs. S1 and S2). ClustalW alignments were used to generate homology models using MODELLER 9v8 software following similar procedure as reported in our previous study [39]. 100 structures were generated and ten best modeled structures were selected on the basis of dope score, and RMSD with respect to crystal structure. The quality of these models was further analyzed with Errat plot and their dihedral angle distributions were analyzed using Ramachandran plot (Figs. S4 and S5). Ramachandran plot of human P-gp homology model generated using mitochondrial P-gp as a template (Fig. S4) showed two residues in the disallowed region. The overall quality factor of homology model was 94.91% in Errat plot. Ramachandran plot of human P-gp homology model generated using Sav1866 as a template (Fig. S5) showed four residues in the disallowed region. The overall quality factor of homology model was 89.91% in Errat plot.

3.2. MTMD

MTMD simulations were performed to incur a better understanding of P-gp translocation mechanism. The technique could be utilized to transform inward open structure of P-gp to outward open through specified intermediate structures. MTMD is a unique technique in which important intermediate catalytic structures could be sampled out, as the P-gp structure transforms from IO to OO state. A quantitative analysis of conformational changes occurring at drug-binding site could be performed and a better understanding of conformational changes responsible for the loss of stable binding interaction of substrate in OO state could be obtained.

The human P-gp homology model generated from *C. elegans* P-gp template was taken as starting structure for MTMD simulation. The IIO state and OO state models generated using human mitochondrial P-gp and Sav1866 P-gp templates, respectively, were taken as targeted structures. The coordinates of IO state model were forced to IIO state and then to OO state using residue mask and applying force constant proportional to difference between RMSD of reference and target structure. During simulation it was observed that the NBDs gradually

approach each other and finally dimerize in OO state forming a catalytic dyad. When viewed from intracellular side, stretching of TM helices can be noticed in correspondence to NBD movements. It appeared as the NBDs were pushing TM helices in a specific pattern, finally exposing the drug-binding region to extracellular space. From extracellular view, it can be clearly observed how pliers like the action of NBD result in opening of TMDs in a specific pattern; not the two TMDs move apart, rather parts of each move apart. The TM1 and 2, of TMD1 and TM9, 10, 11, and 12 of TMD2 move apart from TM3, 4, 5, and 6, of TMD1 and TM7 and 8, of TMD2 (see supplementary information, Movie 1). The MTMD trajectory was quantitatively analyzed for shifts in TMDs, ICH movement in conjunction with NBDs, and stretching in TM helices corresponding to ICH and NBD movements. The placement of ATP-Mg^{2+}-H_2O at NBDs supported alternating site mechanism of ATP hydrolysis [60]. As per recent study of Oldham and Chen [61] that strongly supported the general base ATP hydrolysis mechanisms, ATP-Mg^{2+}-H_2O complex was first placed in NBD1 and ADP and Pi at NBD2. The structure was stable and complex formed stable binding interactions with E556. Subsequent MD trials were also conducted placing ATP-Mg^{2+}-H_2O complex at both NBDs and, ATP-Mg^{2+}-H_2O complex at NBD2 and ADP at NBD1, but none gave stable conformation. Similar observations were also reported in another simulation study conducted by Wise [62]. All further simulations were carried out placing ATP-Mg^{2+}-H_2O at NBD1 and, ADP and Pi at NBD2. Moreover, the conformational changes occurring at drug-binding site during the course of simulation, and the corresponding distance and angular changes in drug-binding residues were also analyzed. Interestingly, we noticed a correlation between conserved apical interactions and NBD movement. The hydrophobic substrate gates were also observed during the course of MTMD simulation. Furthermore, MTMD simulations of substrates and inhibitors gave important insights into their molecular interaction differences during the structural transition of P-gp.

3.2.1. Movement of NBDs and intracellular coupling helices (ICHs)

Before discussing the movements of NBDs during MTMD simulations, it is worthwhile to mention the communication links between NBDs and TMDs. There is a single physical linkage between each NBD and TMD, viz. a loop region (D398-K418) connecting TM6 of TMD1 with NBD1 and another loop region (K1064-G1083) connecting TM12 of TMD2 with NBD2. The other possible communications are non-bonded interactions between NBD and ICH. Out of four ICHs, the ICH1 and ICH4 form a ball and socket like joint with NBD1 and, ICH2 and ICH3 form ball and socket like joint with NBD2 (Fig. 1). These ICH forms conserved salt bridge and H-bonding interactions with corresponding residues in NBDs. ICH1 is a short helix between TM2 and TM3 that insert into the groove of NBD1 near Walker-A region and form close contact with A-loop. ICH3, a short helix between TM8 and TM 9, position itself into the groove of NBD2. ICH2 and ICH4 are short helices between TM4 and TM5, and TM10 and TM11, respectively. These helices are inserted into the groove of opposite half NBD formed by the three subdomains; ATP binding core subdomain (blue), beta-subdomain (wheat) and helical motif (red) (Fig. 1). A detailed list of ICH residues interacting with different parts of NBD and TM helices is provided in Table S3.

As the simulation progressed the separation between NBD1 and NBD2, measured with respect to conserved glutamate residues (Glu 556 and Glu 1201) reduces from 39 Å in IO state to ~14 Å in OO state. Interestingly, it was observed that the NBDs do not follow a straight line path as they approach each other rather they rotate with respect to each other. Fig. 2 represents the movement of NBD during the course of MTMD simulation. In the initial stage of IO to IIO transition the NBDs showed a twisting movement.

The ICHs showed a concerted movement with NBDs. As ICH moved along with NBD it was noticed that most of the conserved interactions between NBD and ICH maintained during IO to IIO state transition of P-gp structure. The conserved salt bridge interactions between Arg 905 (ICH4), Asp 164 (ICH1) and Tyr 444 (NBD1), and that in between Arg 262 (ICH2), Asp 805 (ICH3) and Tyr 1087 (NBD2), disrupted gradually as the simulation progressed from IIO to OO catalytic state (Fig. 3). This was due to the rotation of ICH1 and ICH4 by ~20°and ~82°, respectively, about their horizontal axis (Fig. 4A and B). ICH3 and ICH2 also showed a rotation of ~30° and ~46°, respectively, about their horizontal axis (Fig. 4). During the course of simulation the ICH2 and ICH4 also showed a pivot of ~30° about their vertical axis. Fig. 3 depicts the ball and socket-like movement of ICHs during the course of simulation. Initially, in IO state the ICHs were well fitted into the corresponding grooves of NBDs and as the simulation progressed they rotated into the groove occupying their original position. This combined rotator and translator movements of ICHs prompted us to investigate the relative effects of their movements on the connected TM helices.

3.2.2. Rearrangements in TMDs

The rearrangements in TMDs resulted not only due to translatory motion of NBDs, but also due to rotatory motion of NBDs. In depth analysis revealed that the separation of TMDs occurs in a specific pattern, which resulted due to the arrangement pattern of TMs (Fig. 5), i.e., (i) TM4 and 5 of TMD1 interact with NBD2 and TM10 and TM11 of TMD2 interact with NBD1, (ii) TM6 and TM12, which form physical linkage with NBDs, connects to their respective NBD intersecting the inverted "V" formed by TM3 and TM4 (in case of TM6), and TM9 and TM10 (in case of TM12). Thus, as the NBD moves close, accompanied

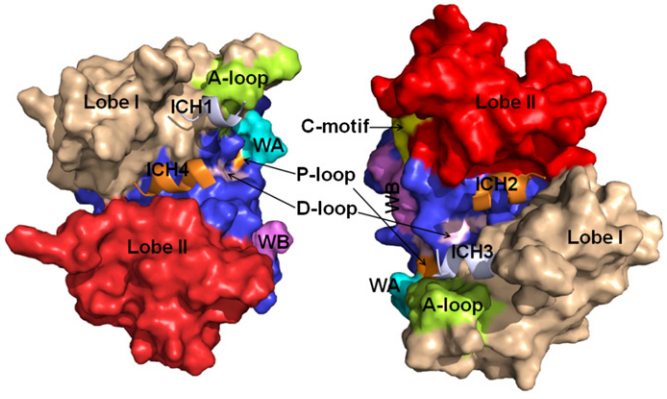

Fig. 1. Arrangement of ICHs on NBDs, ICH2 and ICH4 are arranged in the grove formed by lobe 1 [ATP binding core subdomain (blue) + beta-subdomain (wheat)] and lobe 2 [helical subdomain (red)]. The color coding of other conserved region are: A-loop—green, Walker-A—cyan, P-loop—orange, Signature/C-motif—yellow, Walker-B—violet.

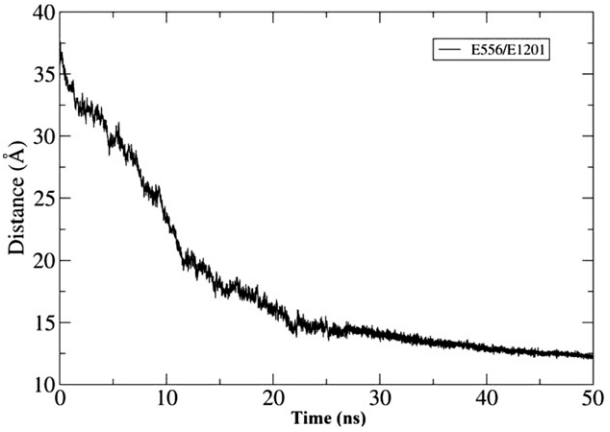

Fig. 2. Distance between two NBDs measure with respect to distance between Cα-atom of conserved residues E556 and E1201.

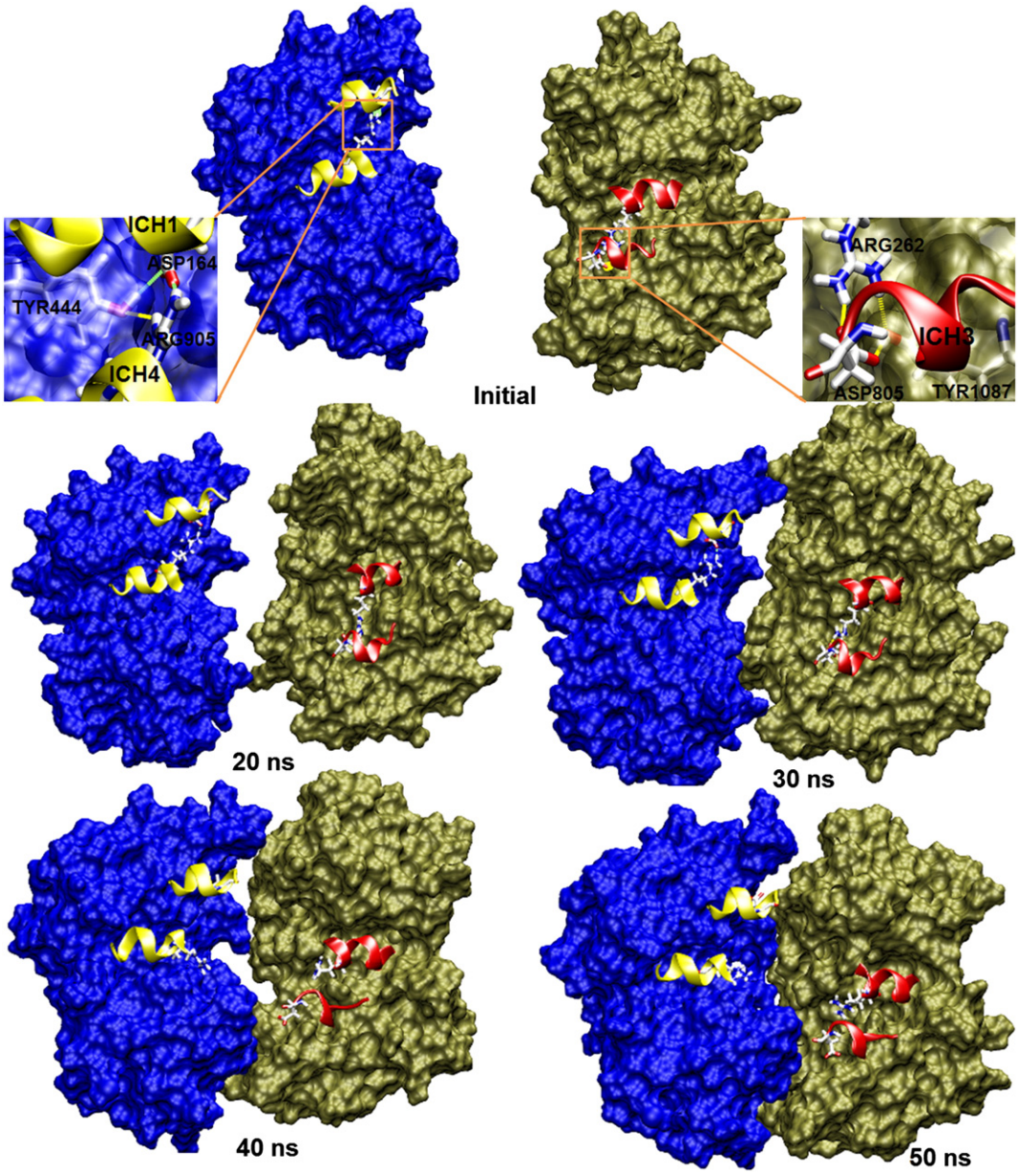

Fig. 3. The conserved salt bridge interactions between Arg 905 (ICH4), Asp 164 (ICH1) and Tyr 444 (NBD1), and that in between Arg 262 (ICH2), Asp 805 (ICH3) and Tyr 1087 (NBD2). These interactions remained intact till IIO conformational state (4 ns), then disrupted gradually as the simulation progressed from IIO to OO catalytic state.

with their twisting motion, the stretching of these TM results into the opening of the TMDs in a plane perpendicular to the movement of NBD.

A quantitative investigation of movements in TMs helices was performed. The distance between adjacent TMs, and TMs facing each other in the two TMDs were plotted during the course of simulation. Figs. 6, 7 and 8 (also see supplementary Fig. S6 for the top view from extracelluar side) depict the separation between different TMs during the IO to OO conformational change of P-gp. Three types of distance plot were plotted: (i) distance between top residues (residue toward extracellular region) of the TM helices (ii) distance between bottom residues (residue toward NBD on helix) of TM helices and (iii) distance between center of mass (COM) of the TM helices. The distance of TM1 was measured with respect to TM2 and TM7, as TM2 is adjacent to TM1 and TM7 was in front of TM1. The initial distance between W55 (bottom residue, TM1) and V711 (bottom residue, TM7) was ~64 Å in IO state, which changed to ~51 Å in OO state (Fig. 6A). Similarly, the distance between E86 (top residue, TM1) and V736 (top residue, TM7) changed from ~16 to 35 Å. In contrast, when the COM distance between TM1 and TM7 was plotted, no noticeable change was observed, this indicated that the TMs moved around a fixed point analogous to a lever/pry-like action. The distance between TM1 and TM2 decreased, and the top residues (E86, TM1 and L107, TM2) moved from ~14 Å to 7 Å, while the bottom residues (Y55, TM1 and R157, TM2) moved from ~32 Å to 27 Å (Fig. 6B). Similar trend was noticed for TM1–TM2 COM movement (moved closed by ~4 Å), indicating that TM1 moved along with TM2 in same direction. A large body of conformational rearrangement was noticed in case of TM2 and TM3, the helices that were also connected to ICH1. The top residues (L107, TM2 and R210, TM3) moved apart from ~23 Å to 33 Å, while the bottom residues (R157, TM2 and V158, TM3) came close from ~23 Å to ~17 Å (Fig. 6C). An approximate separation of 4 Å was observed between COM of both helices. This particular rearrangement was only possible if there was a twisting motion along with translatory motion between two helices; implicating the angular rotation of ICH1 and twisting of NBDs. The movement between TM7 and TM8 was similar to that of TM1 and TM2. Both, TM7 and TM8 showed concerted movement in same direction, the

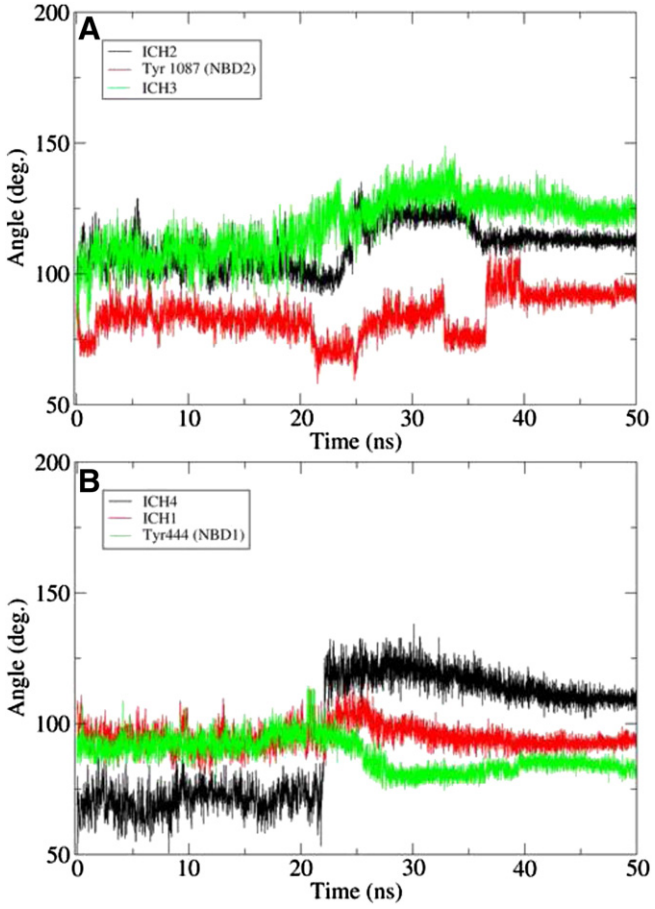

Fig. 4. Changes in angles between Cα-atoms of ICH residues and NBD residues. (A) angular rotation between Cα-atoms of ICH2, ICH3 and NBD2 residues Arg 262-Thr 263-Val264 (black), Asp 805-Asp 806-Pro 807 (green) and Tyr 1087-Asp 1088-Pro 1089 (red), respectively. (B) angular rotation between Cα-atoms of ICH4, ICH1 and NBD1 residues Arg 905-Thr 906-Val 907 (black), Asp 164-Val 165-His 166 (red) and Tyr 444-Asp 445-Pro 446 (green), respectively.

distance between top residues (V736, TM7 and T745, TM8), bottom residues (V711, TM7 and Q797, TM8) and COM changed by ~2 Å (Fig. 7A). Similar to TM2 and TM3 connected to ICH1, TM8 and TM9 were connected to ICH3, which form non-bonded contacts with NBD2. The distance between COM and bottom residues (Q797, TM8 and L812, TM9) changed by ~3 Å, whereas the distance between top residues (T745, TM8 and W853, TM9) increased by ~15 Å (Fig. 7B). This implicated the angular rotation of ICH3 and twisting of NBDs, similar to that noticed in case of TM2 and TM3.

As per the reported experimental data, TM2, TM3, and TM8 do not participate in ligand binding and their conformational changes observed during IO to OO transition of P-gp structure may not affect ligand binding, but their movement and conformational changes had a major contribution in TMD rearrangement cascade. The residues on TM4, TM5, and TM6 of TMD1, and TM9, TM10, TM11 and TM12 of TMD2 that face toward the hydrophobic cavity of P-gp structure in IO state have been reported to participate in ligand binding (list of these residues is provided in supplementary information, Table S2). Further, the movements of these TMs were analyzed. During the IO to OO catalytic state transition of P-gp structure, prominent changes in distance and conformations were observed between T4 and TM10, TM5 and TM11, and TM6 and TM9. Initially, the bottom residues (A259, TM4 and V905, TM10) of TM4 and TM10 had a separation of ~44 Å in IO state, which decreased to 22 Å in OO state (Fig. 7C). Similarly, the bottom residues of TM5 and TM11 came close by ~22 Å (Fig. 8A). Moreover, TM4 and TM5 and TM10 and TM11 are connected to ICH2 and ICH4, respectively; their movements could be directly correlated to the movements of both the ICHs. TM6, which is directly connected to NBD1, and TM9 connected to ICH3 also showed a decrease from 45 Å to 25 Å between their bottom residues (I368, TM6 and L812, TM9) (Fig. 8B). TM6 and TM12 are TM helices physically connected to NBD1 and NBD2, respectively, and their movements directly correspond to the movements in NBDs. The initial separation between bottom residues (I368, TM6 and K1012, TM12) of these TMs was ~52 Å in IO state, which gradually decreased to ~38 Å in OO state (Fig. 8C). A similar study performed by Wise [62] using muring, Sav1866 and MsbA as target structures provides valuable insights into P-gp efflux mechanism and TMD rearrangement. We further tested our simulation protocol by simulating similar targets. The results obtained were similar to those reported by Wise. This further validated our simulation protocol. Fig. S7 provide a comparison of both MTMD simulations. However, both the simulations provide similar insights in TMD rearrangement, but the murine crystallographic structure has been reported to have certain register errors which may raise concerns regarding the drug-binding residues lining TM4 and TM5 (discussed further in text).

On collective observation of distance plots between the TM helices involved in ligand/drug binding, it was inferred that in most of the cases the change in distance between the top residues and COM was less pronounced as compared to the bottom residues. Thus, there were no major displacements in the upper half of these helices as compared to lower one. Therefore, it indicates that along with displacements, the conformational changes in the residues in these TMs majorly contribute to the loss of ligand/drug binding at drug-binding site in OO state.

Further, to analyze the displacement of individual TM helix, RMSD of each TM was plotted. Fig. 9 depicts the RMSD plots of TM helices. The RMSD plots revealed that TM1, TM3 and TM4 of TMD1 (Fig. 9A), and TM9, TM10 and TM12 of TMD2 showed higher RMSD (Fig. 9B).

3.2.3. Conformational changes at DBS and correlation with biochemical and biophysical data

Many efforts have been made to date to characterize the DBS of P-gp. A significant amount of studies have been performed by Loo and Clarke [42–45,49,52,54,55,63], and some other important were those published by Dey et al. [64], Pascaud et al. [65], Shapiro et al. [66] and Lugo et al. [67] Loo and Clarke used cysteine or arginine scanning mutagenesis [49,52] to identify drug-binding residues. In these studies they identified seven residues protected by verapamil. A novel approach of arginine scanning mutagenesis was used by Loo and Clarke to locate residues in P-gp structure that faced toward DBS. These studies were

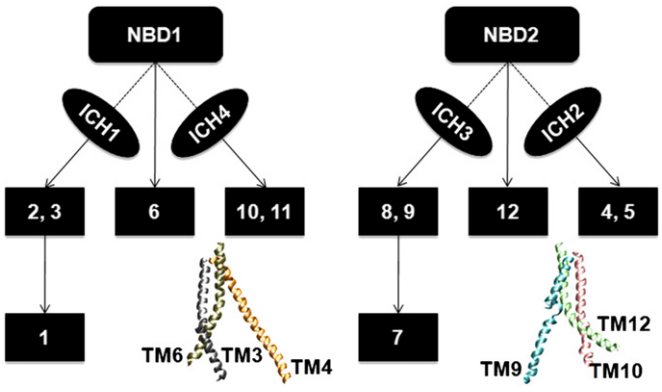

Fig. 5. Arrangement pattern of TMs (number shown in rectangular box) and type of linkage between TMs and NBDs. Solid blue line indicate physical linkage via loop region and dotted red line indicate linkage through non-bonded interactions. The image in cartoon representation shows how inverted V like structure formed by TM3 and TM4, and TM9 and TM10 is intersected by TM6 and TM12, respectively.

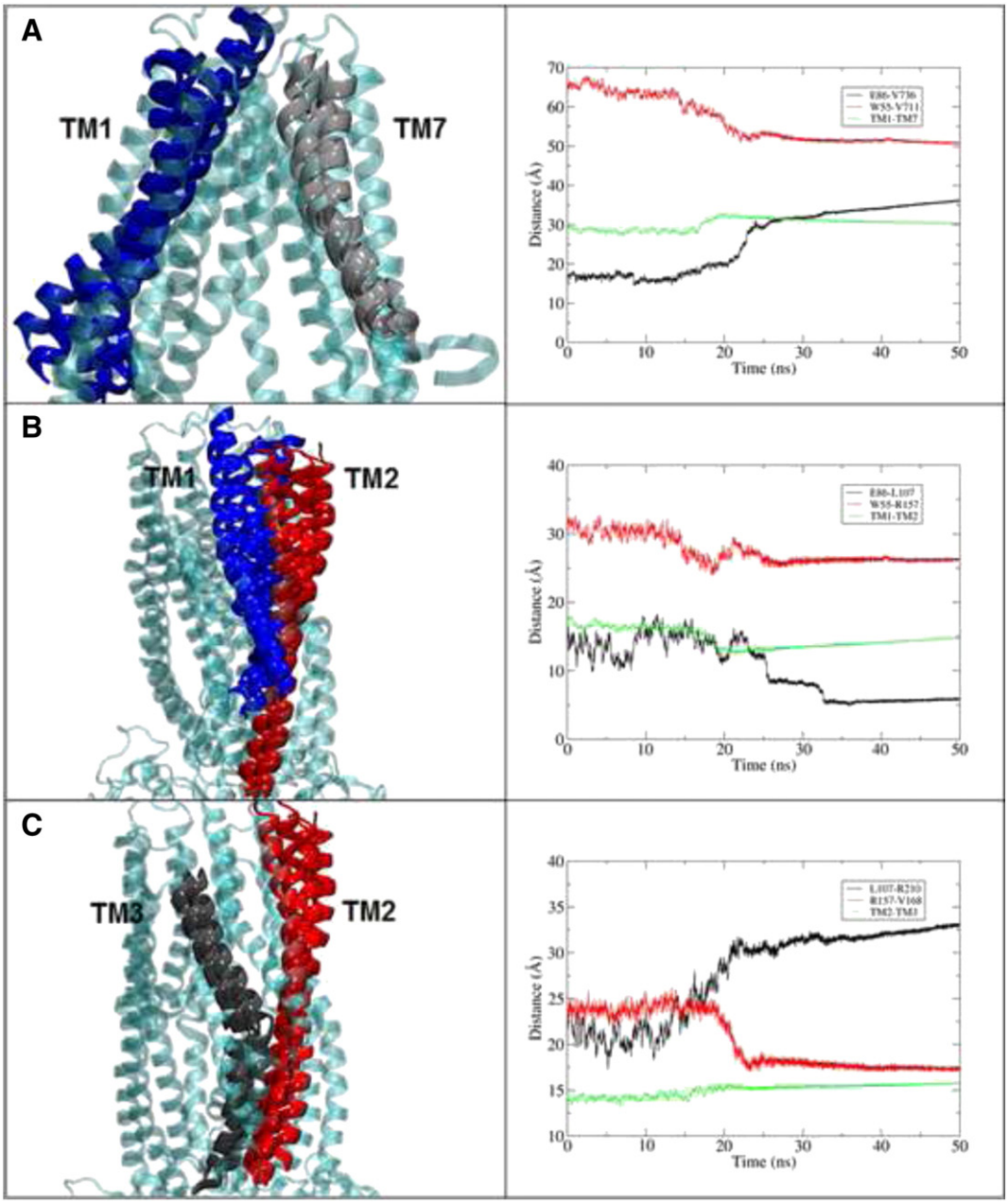

Fig. 6. Relative displacements in TM helices from IO to OO structural transition, initial IO conformation is represented as transparent blue ribbon. The adjacent distance versus time plot shows the quantitative data of the corresponding TM helices during MTMD simulation. A, B and C represent displacements in TM1 and TM7, TM1and TM2, and TM2 and TM3, respectively.

based on rescuing of P-gp folding upon mutation as the bulky arginine side chain, when present in the drug-binding site, mimicked the rescue of folding of certain mutations by transport substrates. Another, 16 residues were identified using dibromobimane studies [44,45,52]. Thio-reactive rhodamine B analog and MTS-verapamil studies were used to identify residues on TM5 and TM6 [55]. On the basis of studies conducted by Dey et al., Pascaud et al., Shapiro et al. and Lugo et al. it may be proposed that P-gp has four binding sites. All drug-binding residues, those identified by Loo and Clarke, Aller et al. [13], Jin et al. [14] and the authors mentioned above were analyzed for their location and respective conformational changes in drug-binding site.

The reported studies depicted that the drug-binding residues were distributed on TM1, TM4, TM5, TM6, TM7, TM9, TM10, TM11 and TM12 in the hydrophobic cavity of P-gp. The generated model was consistent with these biochemical data. The MTMD trajectories were analyzed with the aim to find out the conformational changes and displacements occurring in these drug-binding residues that rendered loss of stable substrate binding interactions. The movements of these residues during the course of simulation are shown in supplementary information Movie 2. Fig. 10 shows the displacements and conformational changes occurring in the drug-binding residues. The progressive changes in the conformation of these residues are indicated using color coding (yellow, orange, gray, red and blue; yellow → orange corresponds to IO → IIO transition; and orange → gray → red → blue corresponds to IIO → OO transition). In the initial IO state the drug-binding residues were facing the hydrophobic cavity and had an optimal conformation for substrate binding. As the simulation progressed from IO to IIO state major displacements in the position of drug-binding residues were noticed (Fig. 10). The structural transition from IIO to OO state was the major transition phase in which substantial conformational changes were noticed that would affect substrate binding. On viewing the movement of these residues from the intracellular side one can notice the residues move away from central axis, finally becoming accessible from extracellular space. On observing the lateral view of

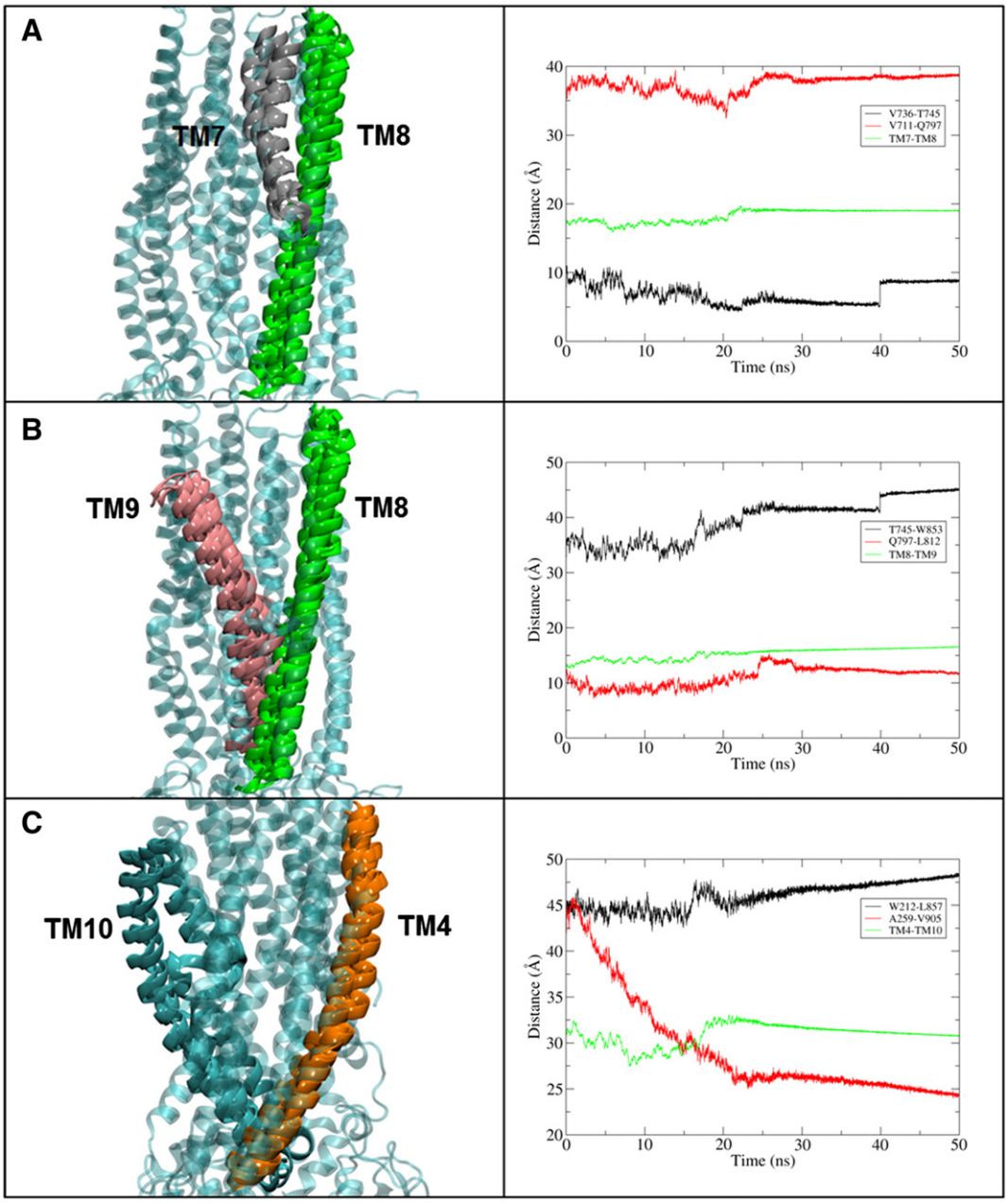

Fig. 7. Relative displacements in TM helices from IO to OO structural transition, initial IO conformation is represented as transparent blue ribbon. The adjacent distance versus time plot shows the quantitative data of the corresponding TM helices during MTMD simulation. A, B and C represent displacements in TM7 and TM8, TM8and TM9, and TM11 and TM12, respectively.

the structural transition (shown as magnified images), it was noticed that the TMs were accompanied by stretching movements. The TM stretching was observed in all TMs but it was more pronounced in case of TM4, −5, −6, −10, −11 and −12. Initially for L65 on TM1 no significant displacement was noticed but as the simulation progresses from IIO to OO state the conformation of Leu residue changes (orange → gray → red → blue) and it faces away from hydrophobic cavity. The S222 residue on TM4 clearly indicates that both stretching and displacement was observed in TM4 but there was no major change in the conformation of Ser residue. Similar movements were noticed for I306 on TM5. In case of L339, I340 and F343 on TM6 stretching movements were coupled with major conformational changes of these residues. The F728 residue on TM7, implicated in verapamil binding showed substantial change in the orientation of phenyl ring, which finally results in loss of stable interaction in OO state. The residues on TM10 (I868 and G872) showed a large displacement and conformation change, the Ile residue rotated by ~60° about vertical axis during the course of transition from IIO to OO state. The F942 and T945 residues on TM11 also showed a substantial displacement from the initial position (yellow, IO state) as the structure transformed to OO state. The F942 residue that forms hydrophobic interactions with substrate showed a high degree of conformational change. In case of TM12, more pronounced conformational changes were observed. It was clearly noticed that the residues L975, V981, V982 and A985, which faced the hydrophobic cavity in IO state, rotated along the vertical axis and attained a conformation in OO state that faced away from hydrophobic cavity.

Cysteine scanning mutagenesis experiments performed by Loo and Clarke [46,47] on IO state of P-gp structure provide important structural information about the relative position of different parts of the TM domains. The consistency of the IO state model with these studies has been proven in our previous study [39]. The TM residues that have

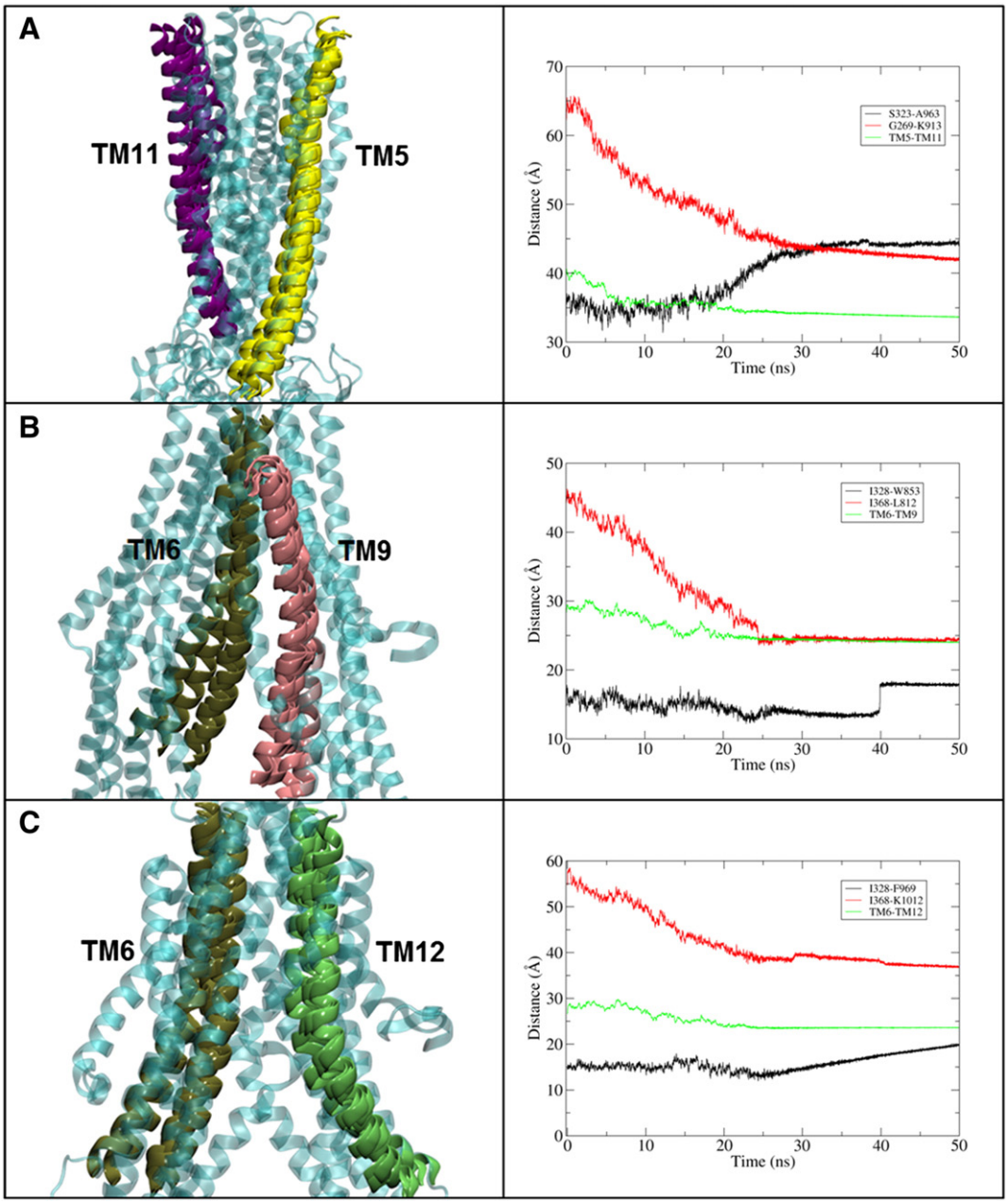

Fig. 8. Relative displacements in TM helices from IO to OO structural transition, initial IO conformation is represented as transparent blue ribbon. The adjacent distance versus time plot shows the quantitative data of the corresponding TM helices during MTMD simulation. A, B and c represent displacements in TM5 and TM11, TM6and TM9, and TM6 and TM12, respectively.

been implicated to form disulfide bond upon cysteine mutagenesis were shown to be located in close proximity in the modeled structure. It was shown using in silico cysteine mutation that the residues of TM2 (Val 133, Cys 137, Leu 138) and TM11 (Gly 939, Ala 935) had inter-residue sulfur distance ranged from 3.3 Å to 5.2 Å, which was within the prerequisite for disulfide bond formation. Similar interactions were shown for TM8 (Phe 766, Phe 770, Phe 771, Gly 774, Phe 775) and TM5 (Gly 300, Ile 299, Ile 297, Asn 296, Ile 293) residues.

Loo and Clarke also established the experimental evidences implicating that the transmembrane helices undergo relative movement during ATP hydrolysis. In a series of cysteine cross-linking studies [48,51,56] they showed that TM helices 11 and 12, 1 and 11, and 6 and 12 formed cysteine cross-linking only if the transporter turned via ATP hydrolysis.

The MTMD simulation trajectories were also analyzed to find out the movement of these TM helices and the residues implicated in cross-linking studies. The distance plot of these residues is shown in Fig. S8. As the simulation progressed from IO to IIO conformation state, the separation between these residues increased, maximum separation was noticed at IIO state (at ~25 ns). Further, as the simulation progressed from IIO to OO state, the transition showed minimum separation between these residues and finally the separation increased as the OO conformation state was achieved (at ~40 ns).

In a recent study, Loo and Clarke [58] provided biochemical evidence that the structure of ICH2 in human P-gp resembles the crystal structure of *C. elegans*, rather than that of mouse P-gp. The homology model of human P-gp based on mouse P-gp erroneously predicts ICH2 residues (residues Val253–Ala259 and Gly269–Lys272) as loop instead of α-helices. The correct conformation of this region can be modeled using *C. elegans* P-gp as template. The major difference between the two models is the conserved salt bridge interaction between Glu256 and Arg276, which is noticed only in *C. elegans*-based homology models.

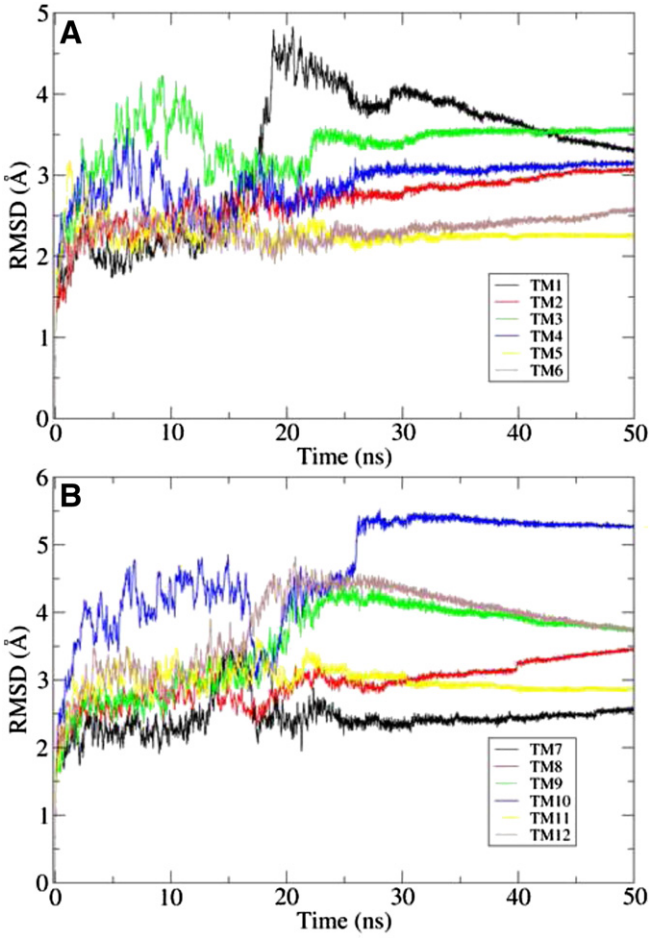

Fig. 9. RMSD versus time plot of TM helices. (A) Plot of TM helices in TMD1, (B) Plot of TM helices in TMD2.

The presence of a salt bridge between Glu256 and Arg276 was found to promote maturation of human P-gp.

The simulation was found consistent with the conserved salt bridge interactions between Glu256 and Arg276. Fig. S9 shows the conserved salt bridge interaction during MTMD simulation. It was noticed during MTMD simulation that the conserved salt bridge interactions maintained from IO to IIO structural transition and disrupted when the transition structure approached closer to OO state.

In another recent study, Loo and Clarke [57] performed drug rescue of P-gp processing mutant experiments containing an arginine at each position in TM5. The experiments help to identify positions of residues facing the lipid or internal aqueous chamber. Correct orientation of TM5 is critical for P-gp-drug binding in silico experiments, since residues in TM5 (particularly I306) have been implicated to play a crucial role in binding of drug substrates and coupling of drug binding to activation of ATPase activity [68]. In their study, the authors showed that the human P-gp homology models based on mouse P-gp predict wrong orientation of I297, G300, A301, L304, A308, and A311 (actually face lipid environment, but predicted to face drug-binding pocket), and A295, S298, A302, L305, I306, and S309 (actually face drug-binding pocket, but predicted to face lipid environment). The developed model was found consistent with the position of these residues (Fig. S10). Thus, corroborates the accuracy of structural modeling and suitability of performing P-gp substrate/inhibitor binding studies on the developed model.

In another recent experiment [69], Loo and Clarke tested the effects of cross-linking mutant L175C (ICL1)/N820C (ICL3) to determine the distance between N-terminal and C-terminal half of P-gp that show high or low ATPase activity. They observed that there was over 10 fold increase in basal ATPase activity when L175C was linked to N820C with cross-linkers predicted to span a distance of less than 20 Å, and predicted that the ATPase activation switch appears to be turned on or off when this distance is less than or greater than 20 Å, respectively. In context to this study, here in our simulation studies we monitored the distance between the L175 and N820 with respect to distance between catalytic important residue E556 and E1201 and movement of NBDs (a video in supplementary information, Movie 3 presents the motion of these residues and NBDs during the course of simulation). It was observed that as the distance between L175 and N820 reduced from initial 29 Å to 20 Å the NBDs showed a twisting movement and came closer. At a point where the distance between L175 and N820 was 20 Å the distance between E556 and E1201 was 21 Å (initial, at IO conformation was 39 Å). During this transition phase the NBDs completed their twisting movement and were properly aligned, ready to form a sandwich dimer thereafter, indicating the possible structural rearrangement in P-gp that resulted in increased ATPase activity when the distance between L175 and N820 decreased below 20 Å separations. Similar type of NBD movement was also observed by Wise [62].

Further, we performed in silico mutation analysis followed by MTMD to get insights into the role of conserved apical interactions between Phe335, Tyr310, Phe314 and Ile218, which is believed to be responsible for the stability of IO conformation of P-gp structure [14,70,71]. The Phe335 was located at the apex of the drug transport pathway, making van der Waals interactions with Tyr310 and Phe314 in TM5, and Ile218 in TM4 (Fig. S11B). Interestingly, it was noticed during MTMD simulation that the movement of NBDs and formation of their catalytic dyad during OO catalytic state, are somehow correlated to these conserved apical interactions in P-gp structure in IO catalytic state. To verify the role of these interactions in P-gp catalytic transformation, these residues were mutated to alanine (Fig. S11C). As a result the binding interactions were disrupted. The mutated structures were again subjected to MTMD simulation. It was observed that the movement of NBDs changed substantially. Figs. S11D and S11E show the movement of conserved Glu residues of NBD before and after mutation, respectively. The twisting movement of NBDs became less pronounced. The graph in Fig. S11F clearly shows that the separation between the Glu residues increased after mutation. Thus, resulting into the distortion of catalytic dyad and may result in loss of activity.

Moreover, the hydrophobic substrate gates were also noticed during the MTMD simulation. These gates were noticed during IO to IIO transition of P-gp structure. The gates were noticed in the hydrophobic membrane embedded region of P-gp. A hydrophobic gate with ~18 Å in diameter was noticed between TM1 and TM2 (constituted by residues Ile 60, Val 125 and Ala 128) and another of ~14 Å in diameter was noticed between TM7 and TM9 (constituted by residues Ala 718, Gly 722, Ala 834 and Ala 841) (Fig. S12). Similar hydrophobic gates between TM1 and TM2 were also noticed by Shintre et al. [10], though the study does not mention any hydrophobic portal between TM7 and TM9. It was noticed during the simulation that the residues Ala 718, Gly 722, Ala 834 and Ala 841 that formed a tight packing close to lipid bilayer in IO conformation gradually move away making an access portal to the cavity of P-gp. Similar transition was also noticed between residues of TM1 and TM2.

3.3. Induced fit docking and MTMD analysis of substrates/inhibitors

This part of study was conducted with an objective to address following queries: (i) to figure out is there different binding site for substrate and inhibitor, (ii) differences in molecular interactions of substrate and inhibitor, (iii) conformational changes in the key residues involved in ligand binding and how these conformational changes render instability in ligand binding, and (iv) efflux motion path followed by substrates and inhibitors. To confer these objectives, eight substrates

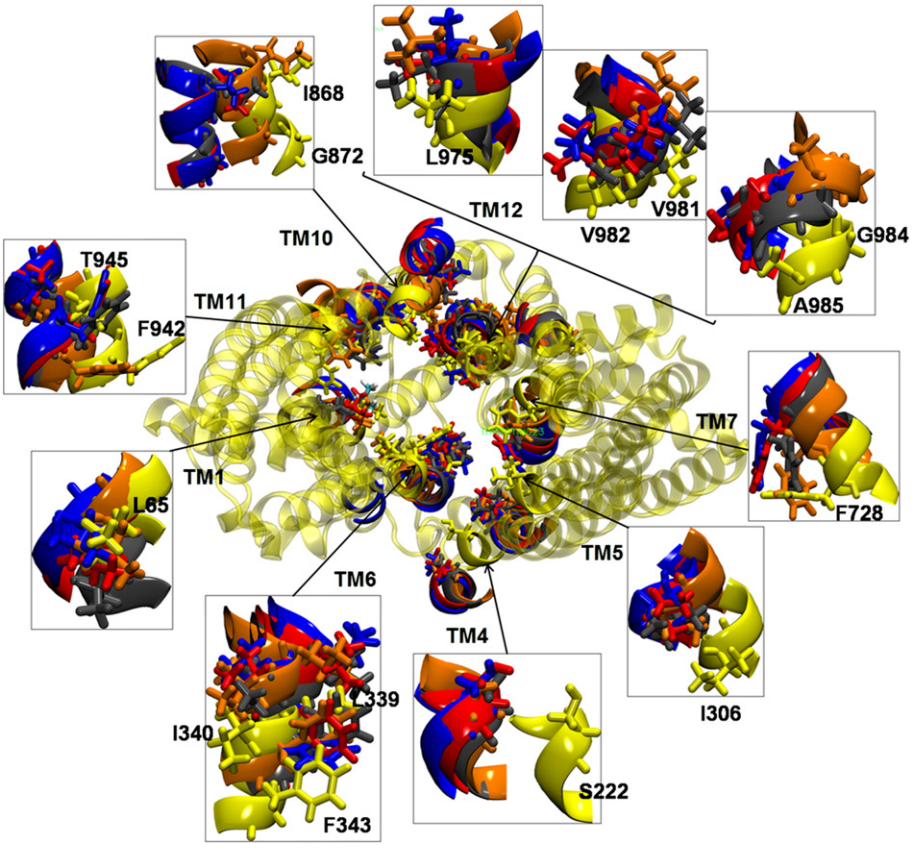

Fig. 10. Conformational changes and displacements observed in drug-binding residues during IO to OO structural transition of P-gp. The figure shows intracellular view of the initial IO conformation state, represented as transparent ribbon (NBDs are not shown). The progressive changes in the conformation of drug-binding residues (magnified lateral view) are indicated using color coding (yellow, orange, gray, red and blue; yellow → orange correspond to IO → IIO transition; and orange → gray → red → blue correspond to IIO → OO transition).

and eight inhibitors of P-gp were subjected to induced fit docking in developed human P-gp homology model. The best docked poses of substrates and inhibitors were then subjected to multi-targeted molecular dynamics to investigate the changes in molecular interactions during the catalytic transition of P-gp.

The IFD protocol was validated as mentioned in the previous work [39] (data not shown). The co-crystallized structure (OSA) was docked into *C. elegans* crystal structure. Interactions and conformation of co-crystallized ligand similar to crystal structure were generated by IFD, forming H-bonding interactions with Thr 1025 and Thr 1028, and having an atomic RMSD of 0.68 Å. IFD in human P-gp homology model also showed interaction with homologous residues. Further, IFD studies of known P-gp substrates and inhibitors (listed in supplementary information Table S1) were performed on human P-gp homology model.

The in-depth investigation of IFD poses showed that the substrates and inhibitors formed stable binding interactions with the experimentally reported residues. The first row of each entry (labeled as initial) in Table S4 and S5 enlists the residues that were in close contact with respective inhibitor and substrate. 3D interaction images of each substrate and inhibitor are provided in Figs. S13–S25. Each substrate and inhibitor formed stable binding interactions with at least three of the experimentally reported residues except nifedipine. The docking of co-crystallized substrate and the stable binding interactions of test compounds well correlated with the experimental studies [42–45,49,52,63,64,67]. Thus, the results strongly supported the validity of docking experiments and structural modeling of human P-gp.

In context to first objective no separate binding sites were observed for substrate and inhibitor. Two binding sites were noticed viz. one accommodated between TM4, TM5, TM6 TM7, TM8 TM9 and TM12 (site 1) (Fig. 11A) and other between TM1, TM2, TM3, TM6, TM10, TM11 and TM12 (site 2) (Fig. 11B). Both sites had TM6 and TM12 in common, which have been proved to be involved in ligand binding through experimental studies [45,49]. Both substrate and inhibitor showed binding tendency in either of the active site. The test substrate *etoposide* occupied stable docked conformation in site 1, whereas the other test substrate showed stable binding conformation at site 2 (substrates/inhibitors occupying site 1 would be written in italics further in text for easy distinction). However, in case of inhibitor about half of the inhibitors occupied site 1 (*biricodar*, *tamoxifen*, *tariquidar and verapamil*) and the other half occupied the site 2 (laniquidar, nifedipine, reserpine and ketoconazole). Tables S4 and S5 clearly indicate that most of the substrates and inhibitors have common interacting residues. Analyses concerning the difference in molecular interactions between substrate and inhibitor, each compound had varied interactions depending upon its molecular structure and property, but no clear distinction between the interactions of substrates and inhibitors was noticed. Hydrophobic interactions were predominantly responsible for stable binding in most of the cases.

Moreover, as discussed in a study conducted by Loo and Clarke [72] binding of substrate induces conformational changes in TM helices. In IFD experiments substrate and inhibitor induced conformational changes in the residues of TM helices were noticed. For instance, doxorubicin showed conformational changes in residues of TM helices (Fig. S26A). The residues P350 (TM6) and S993 (TM12) were reported to cross link in the cysteine mutagenesis experiments, the distance between these residues increased in response to doxorubicin binding. The residue V991 (TM12) shown to cross link with P350 due to substrate (colchicines/demecolcine) induced conformational changes, was

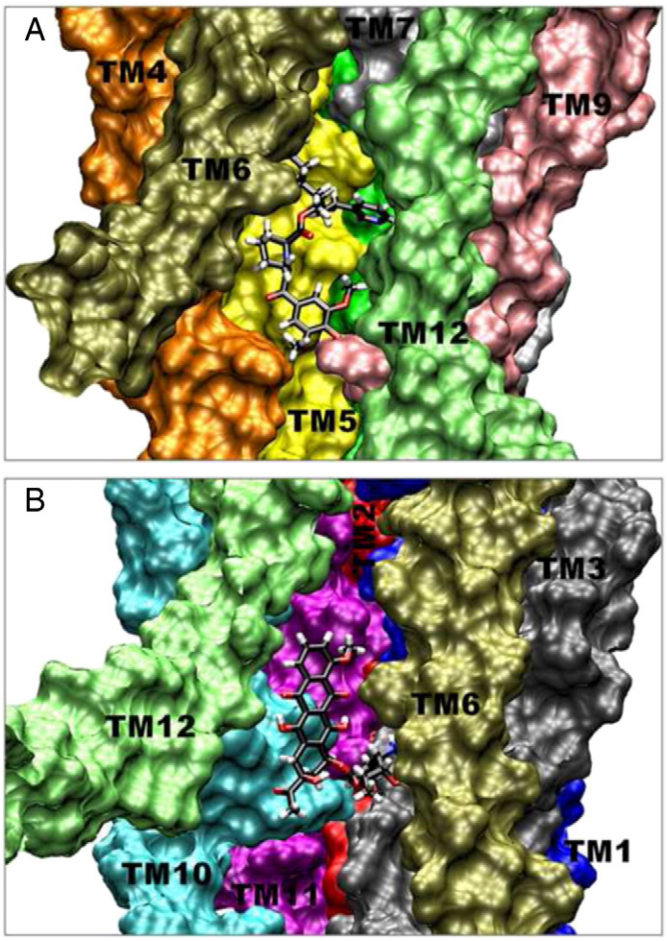

Fig. 11. The two binding sites observed during induced fit docking studies. (A) Site 1, accommodated between TM4, TM5, TM6 TM7, TM8 TM9 and TM12. (B) Site 2, accommodated between TM1, TM2, TM3, TM6, TM10, TM11 and TM12.

observed to move closer to P350 in response to doxorubicin binding, indicating the possible reason of cross linking observed due to substrate induced conformational changes. Similar conformational changes were observed for all anthracycline compounds (Fig. S26B). The study reported, no cross linking was observed in any mutants in case of verapamil and vinblastine, however conformational changes in residues were observed in response to verapamil and vinblastine binding. The possible reason why cross-linking was not observed could be; (i) in case of vinblastine it was observed that the residues V991 (TM12) and S993 (TM12) both moved away from P350 (Fig. S26C) and (ii) in case of verapamil it was observed that verapamil binds at site 1, which do not involve TM11, and its binding induced major conformational changes in the residues of TM5, TM6 and TM12 (Fig. S26D), moreover the residues P350 and S993 were not in the vicinity of verapamil binding.

MTMD studies of stable binding poses of substrates and inhibitors were further carried out to analyze the conformational changes in the residues forming stable binding interactions. In depth analyses of conformational changes in drug-binding residues were carried out during the P-gp structure transition from IO to OO catalytic state. Each residue was closely observed to find out the changes in molecular interactions that destabilized the stable binding of substrates and inhibitors. Also, to elucidate the path followed by substrate and inhibitor, while they are effluxed out, and any possible distinction between the two, which differentiate them as substrate and inhibitor. However, the timescale of simulation was insufficient to trace out the actual motion path of substrate and inhibitor; we observed a clear distinction between the molecular interactions of substrate and inhibitor. On analyses of MTMD trajectories it was observed that most of the residues, which have been implicated in ligand binding, face away from the translocation pathway as the structure approaches closer to OO catalytic state. These conformational changes in the drug-binding residues completely destabilized the stable hydrophobic interactions essential for ligand binding. As the transition in P-gp structure proceeds from IO to OO state, the lining of the drug translocation pathway gradually changes from highly hydrophobic to less hydrophobic and finally to hydrophilic. The RMSD plot of each substrate and inhibitor (Fig. 12) clearly indicates that as the P-gp structure enters the IIO to OO transition phase there is a noticeable increase in the RMSD of substrates and inhibitors. It was observed that most of the substrates get destabilized due the conformational changes in the residues lining the drug-binding pocket and dislocates from actual binding site. In Fig. 12B the increase in RMSD corresponds to the dislocation of substrate from the drug-binding site. Similar kind of destabilization was also noticed in inhibitors (Fig. 12A), however the changes in their interactions were different from substrates. Though the inhibitors also dislocated from actual binding site, they seemed to be "sticky" i.e. they showed a tendency to retain stable binding interaction with at least one of the drug-binding residue during the catalytic transition from IO to OO state. Table S4 lists the residues in close contact during each nanosecond of simulation, residue represented in bold (at least one is the drug-binding residue implicated in experimental studies) maintain close contact during all phases of simulation. The table clearly shows that unlike substrate, each inhibitor maintained a close contact with either of the drug-binding residue during all phases of the catalytic transition.

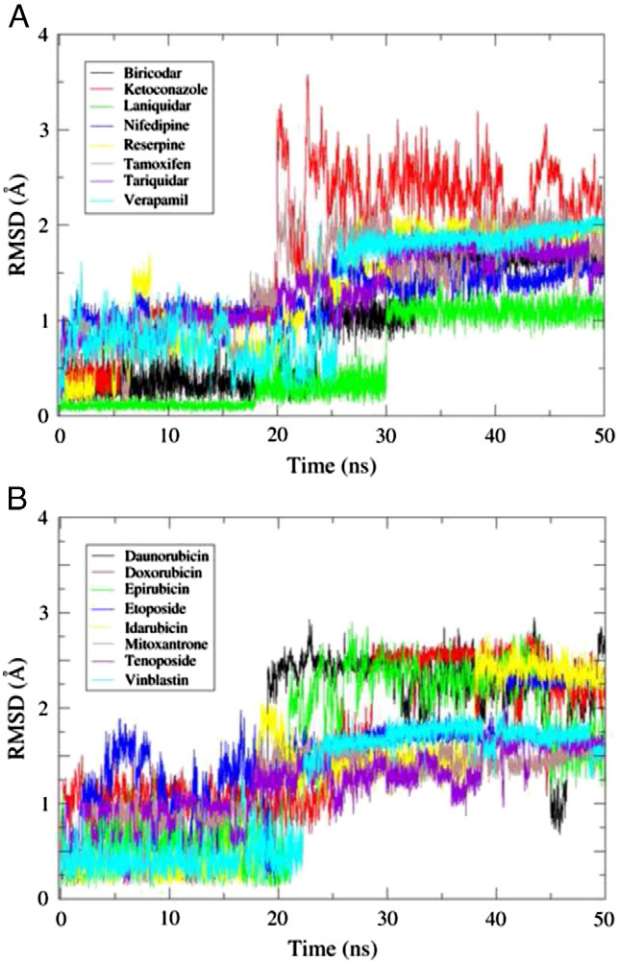

Fig. 12. RMSD plot of compounds during the course of MTMD simulation. (A) RMSD plot of inhibitors (B) RMSD plot of substrates.

Biricodar tends to retain its hydrophobic interaction with I306, A342 and F343, ligand binding residues implicated in experimental studies, during the all transition phase of P-gp structure from IO to OO state. It also maintained close contact with F303 and Y310. Laniquidar maintained close contact with I868. Reserpine maintained its hydrophobic interactions with F942 and A985. *Tariquidar* maintained binding interactions with I306 and F343. *Tamoxifen* maintained hydrophobic interactions with L399, F343 and F728. Ketoconazole retained its interactions with T941 and T945. *Verapamil* maintained hydrophobic interactions with I306, L399, A342, F343 and V982. In contrast, the substrates lost their stable binding interactions after IIO catalytic state and get destabilized, and dislocates from actual binding site. Snapshots of interaction of each substrate and inhibitor during the course of MTMD simulation is provided in supplementary information Figs. S13–S25. The four anthracycline compounds occupied the same binding site (site 2) having almost similar molecular interactions. The change in their RMSD pattern (Fig. 12B) was also observed to be similar as the most of interacting residues were common, the conformational changes in the interacting residues (Table S4) during IIO to OO transition resulted in sudden increase in the RMSD as the compound loses most of its stable interactions. *Verapamil* and doxorubicin as a representative of inhibitor and substrate respectively are discussed in detail.

Initially in IO state, *verapamil* showed stable binding interactions at site 1. Fig. 13 shows the gradual changes in conformation and position of residues that formed close contact with *verapamil*. The close contact residues are shown as licorice (residues implicated in drug binding of P-gp) and CPK representations. *Verapamil* showed hydrophobic interactions with L339, Y310, F343 and I306, and π–π interaction with F303, initially in IO state (Fig. 13A). As the simulation progressed from IO to OO conformation state these interactions changed gradually. When the structure acquired a conformation close to IIO state (Fig. 13B), *verapamil* loses π–π interaction with F303. Fig. 13C represents a transition structure noticed after IIO state (at the beginning of IIO to OO transition), clearly shows that most of the close contact residues (CPK, representation) moved away from *verapamil*, losing their close contacts. However, *verapamil*, though in different conformation maintained hydrophobic interactions with drug-binding residues L339, F303 and Y307, and showed close contact with Y310 and F343. Finally, in OO state (Fig. 13D) *verapamil* showed conformational change, but retained its hydrophobic interactions with drug-binding residues. A video showing these conformational changes in presented in supplementary information (Movie 4).

In contrast, doxorubicin showed stable binding interactions at site 2 in IO state and formed hydrophobic interactions with L65, F343, F942 and M986 (Fig. 14A). Doxorubicin maintained these stable interactions till IIO state (Fig. 14B). As the simulation progressed from IIO to OO state, doxorubicin gradually moved out of the binding pocket losing the stable binding interactions (Fig. 14C). Finally, in OO state (Fig. 14D) both drug-binding residues and the residues in close contact showed maximum separation with doxorubicin, destabilizing the stable binding of doxorubicin. A video showing these conformational changes in presented in supplementary information (Movie 5).

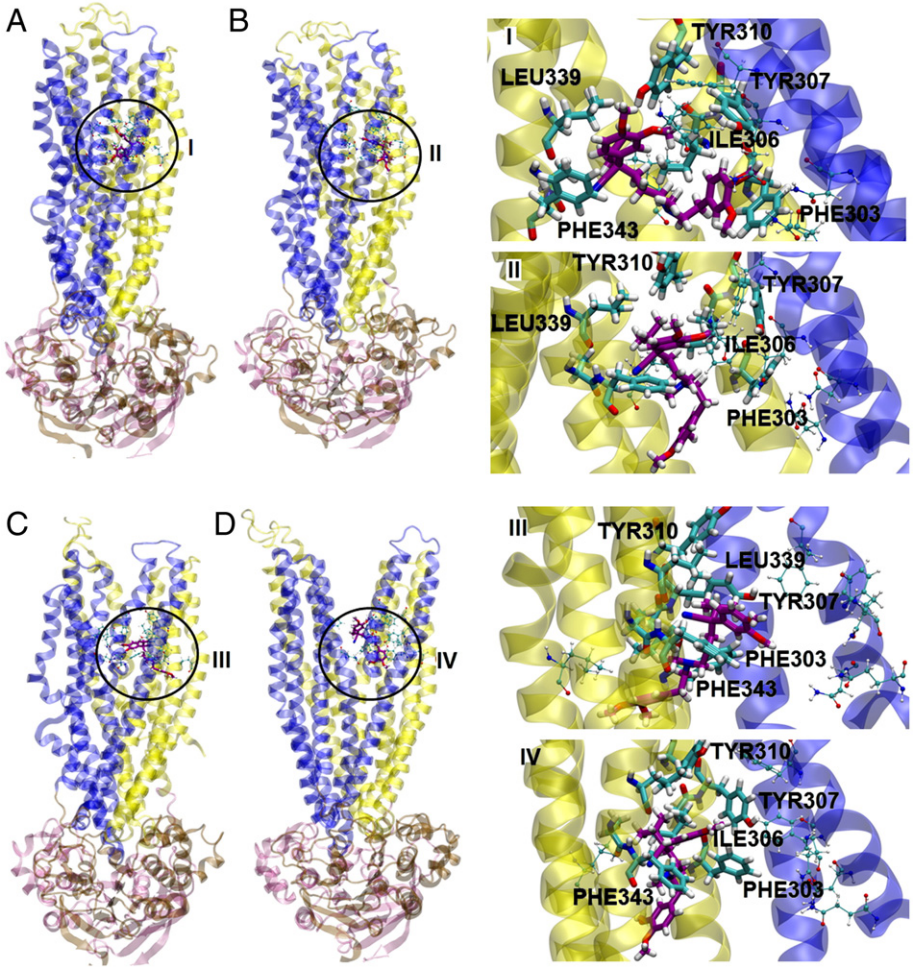

Fig. 13. Changes in molecular interactions of verapamil observed during MTMD simulation; A, B, C and D represent the P-gp transition structures initial IO, at starting of IIO, after IIO and OO conformation state, respectively. The magnified images of encircled region are shown as I, II, III and IV.

3.4. Insights into P-gp translocation mechanism

The MTMD technique used here to study the structural changes in P-gp structure as it transforms from IO to OO catalytic state provided valuable insights into the P-gp efflux mechanism. The TMD analyses, details of NBD movements, and measurements of ICH movement and rotation in ball and socket joint of NBD provide a clear picture how P-gp structure undergoes a large body of structural changes from drug-binding pocket exposed to intracellular space to drug-binding pocket exposed to extracellular space. Also, the specific pattern of opening of P-gp structure to the extracellular space is due to the specific arrangement pattern of TM helices in TMDs.

The ICHs were noticed as main connecting link between TMDs and NBDs and could be regarded as motion transformers that transform the twisting and translatory motion of NBDs to pushing motion. These motion transformers are vital link for P-gp efflux mechanism. During the transition from IO to IIO state the NBDs move closer, the ICHs also move in concert and the translatory shift of NBDs is transmitted to TMDs via ICHs as a pushing motion. ICH1 connected to TM2 and TM3, pushes these TMs as it moves from IO to OO conformation state; however the stretching of both TMs is in opposite direction. This is due to the arrangement of TMs in TMD1. TM3 is connected to TM4 through a short extracellular loop, which in turn is connected to ICH2 embedded in NBD2. Thus, the movement of TM3 is also affected by the movement of TM4. TM4 and TM5 are connected to ICH2 and shows stretching due to a push exerted by ICH2 in response to NBD2 movement. Moreover, TM5 connected to TM6 (has physical contact with NBD1), through an extracellular loop, which intersect the inverted V formed by TM3 and TM4. This arrangement results into the movement of TM3, −4, −5 and −6 toward the same side. So, if one observes the structural change in TMD1 from a lateral view with both NBD overlapping each other, it could be clearly observed that the TM3, −4, −5 and −6 moves in left directions and TM1 and TM2 moves in right direction. Interestingly, the gradual pushing motion of ICH2 on TM4 and TM5 during transition from IO to OO state gradually straightened these helices and finally they attained a bow-like structure in the OO conformation state. However, the curvature was more pronounced in the case of TM4. Similar type of rearrangements was observed in TMD2 in response to pushing force exerted by ICH3 and ICH4, while showing a concerted movement with NBD1 and NBD2. In TMD2, TM10 and TM11 showed a curved bow-like structure in final OO conformational state, TM10 showed more pronounced curvature. These gradual rearrangements in TMD1 and TMD2 from IO to IIO, and then to OO state finally resulted in the opening of P-gp structure toward the extracellular space making the drug-binding region solvent accessible from the extracellular side.

Moreover, the movements of ICHs and the corresponding movements in TM helices observed in MTMD simulation provide a good explanation for the inactivation of P-gp on cross-linking ICH2 and ICH3, mentioned in a recent experimental study [73]. In this experiment Loo and Clarke cross-linked A259C (ICH2) and W803C (ICH3) that resulted in loss of P-gp ATPase activity. The role of ICH discussed above and in the previous section clearly explains that the cross-linking will inhibited the conformation changes in TM4, TM5, TM8 and TM9 in response to ICH2 and ICH3 movement, which possibly explain the reason of P-gp inactivation. The study also discusses the importance of Y1087, mutation in which inhibited maturation of P-gp. In our simulation studies Y1087 was found to form conserved salt-bridge interactions with Arg 262 (ICH2) and Asp 805 (ICH3) in IO conformation, which gradually

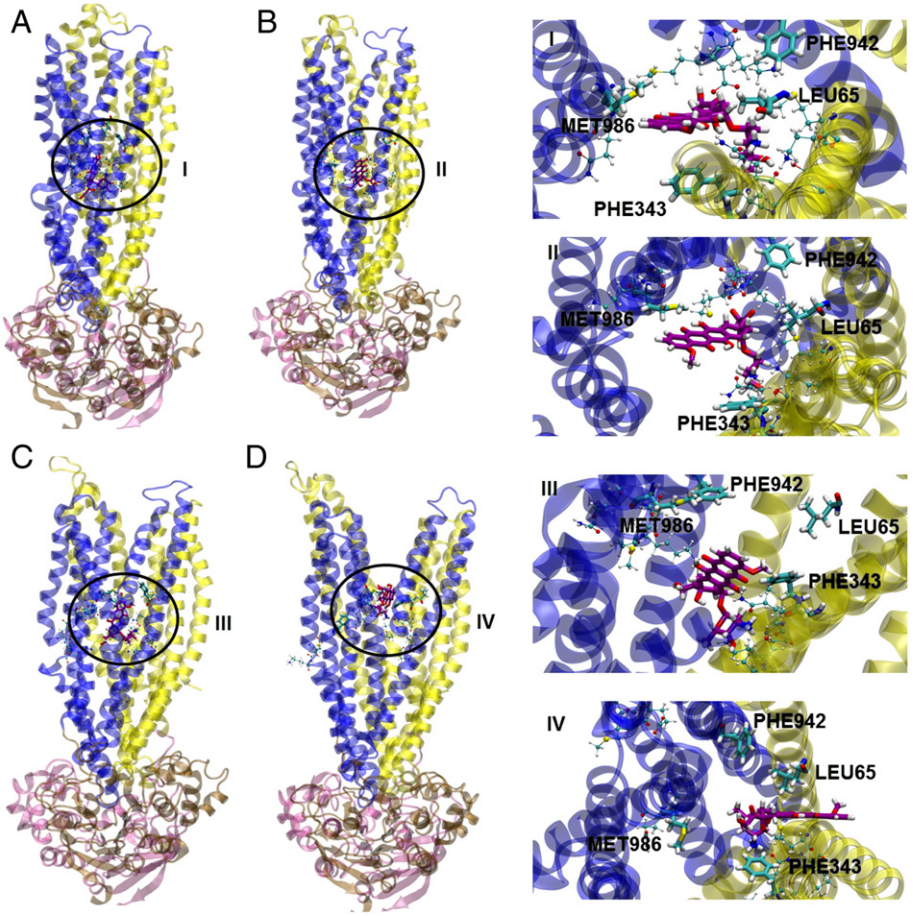

Fig. 14. Changes in molecular interactions of doxorubicin observed during MTMD simulation; A, B, C and D represent the P-gp transition structures initial IO, at starting of IIO, after IIO and OO conformation state, respectively. The magnified images of encircled region are shown as I, II, III and IV.

disrupted from IO to OO transition (Fig. 3). The mutation in Y1087 will not only abolish conserved salt-bridge interaction but also inhibit the related conformational changes in ICH2 and ICH3.

The quantitative data relating movements of TM and ICH discussed in the previous section well correlates with the mechanism hypothesized above on the basis of MTMD experiments. A negligible change was observed in the distance between TM1 and TM2 that indicates both the TMs move in same direction. However, the straightening of TM2 resulted into the conformational change in the extracellular loop connecting TM1 and TM2. This loop is analogous to a lid that covers the extracellular opening of the P-gp transporter. As the TM2 straightens during IO to OO transition this loop gradually moves to open the extracellular covering. The large change noticed in distance between TM2 and TM3 is reasonable as both TMs move in opposite direction. The angular twist of ~20 Å observed in ICH1 could be correlated to provide initial opposite directional momentum to TM2 and TM3 in response to pushing exerted by ICH1. The prominent change in the distance between TM4 and TM10, TM5 and TM11, and TM6 and TM9 was observed as they moved in opposite direction. The higher RMSD of TM4 and the twist in ICH2 could be correlated to higher curvature observed for TM4. The higher RMSD of TM1 as compared to TM7 was attributed to higher conformational change in extracellular loop connecting TM1 and TM2.

The MTMD simulations of substrates and inhibitors gave insights into the structural transition of TM helices. During IO to OO transition the TM helices move away accompanied by conformational changes in the drug-binding residues, in response to these conformational changes both substrate and inhibitor were dislocate from their actual binding site, but the inhibitors seemed to maintain the binding interactions with some of the drug-binding residues. The observed results does not state any quantitative differentiation in binding affinity of substrate or inhibitor, however it could be proposed that in actual biological mechanism inhibitors may have a tendency to inhibit certain conformational changes in these drug-binding residues and thus hindering the movement of TM helices essential for catalytic efflux. Also, it could be interpreted that the inhibitors may have higher binding affinity then substrates.

The translocation mechanism of P-gp proposed here on the basis of MTMD experiments on P-gp structures and large number of MTMD experiments conducted with known P-gp substrate and inhibitors presents an overall picture of P-gp translocation mechanism. The study gives substantial detailed into reaarangements of TMDs, importance of ICHs and interactions of inhibitors during P-gp catalytic providing testable hypotheses for future studies.

4. Conclusions

The selected template structures for modeling studies had a large difference between their NBDs representing different catalytic state of P-gp. The generated human P-gp models in three different catalytic states, using *C. elegans*, human mitochondrial and Sav1866 P-gp as templates showed very few geometric constraints. Ramachandran and errat plot indicated good reliability of generated models. The subsequent embedding of model in lipid bilayer followed by 50 ns MD equilibration further refined the overall geometry of the structures. Furthermore, the models showed good consistency with experimental studies, providing reasonable structures to perform ligand binding interaction studies.

The MTMD technique used here gave valuable insights into the P-gp efflux mechanism. The IO conformational state was taken as the starting structure for MTMD studies, as this structural state was well validated against experimental data. Moreover, the IO to OO structural transition could be better utilized to study substrate/inhibitor binding interactions, as the substrate and inhibitor bind stably in IO conformation of P-gp and later get destabilized in OO conformational state. The MTMD simulation from IO to OO state incurred a better understanding of the NBD movements, role of ICHs and TMD rearrangements during the P-gp efflux cycle. The IO to OO structural change of P-gp is contributed by both twisting and translatory motion of NBDs. The IO to IIO state change showed the initial twisting motion of NBDs, while IIO to OO state transition showed translatory motion where the NBDs approach each other and dimerize to form catalytic dyad. ICHs, which were well adjusted into the grooves of NBDs forming a ball and socket-like joint, showed concerted movement with NBDs. These ICHs were observed as motion transformers that transform rotatory and translatory motion of NBDs to a pushing motion, resulting into the rearrangement of TMDs. Moving along with NBDs, ICHs also showed rotatory motion into the grooves of NBDs as governed by conserved interactions. Coupled with rotatory motion the ICHs pushed 8 out of 12 TM helices (2, 3, 4, 5, 8, 9, 10 and 11), predominant pushing force was exerted on TM4–TM5, and TM10–TM11 via ICH2 and ICH4, respectively. In response to NBD and ICH movement, the TMDs showed a dramatic rearrangement, finally resulting into the opening of drug-binding region to extracellular space. A specific pattern of opening of TMDs was due to the topological arrangement of TM helices. The diametric stretching of TM2 and TM3 in response to ICH1 movement was observed on account of the arrangement of TM3, 4 and 6, and bent topology of TM3 helix. Identical arrangement of TM8, 9 and 12 resulted into the diametric stretching of TM8 and TM9. The stretching TM2 also resulted into the conformational change in extracellular loop connecting TM1 and TM2. Prominent straightening of TM4, 5, 10 and 11 observed during IO to OO structural transition of P-gp in response to ICH2 and ICH4 movements, respectively, majorly contributed to TMD rearrangement.

The study provides significant details of conformational changes in the drug-binding residues that occurred from IO state, where drug-binding pocket is accessible from intracellular space to OO state, where drug-binding region becomes accessible from extracellular space. The simulation clearly depicted that the drug binding-residues acquired conformation that face away from drug-binding pocket as the P-gp structure approached the OO state. Along with conformational changes, these residues also showed displacements from their initial position, gradually moving apart from central axis. The conformational changes in drug-binding residues and their corresponding movements distorted the binding site(s) and represented a clear picture how a stably binding ligand possibly get destabilized in OO conformation state. Furthermore, the consistency of developed model and MTMD simulations with experimental data provide strong evidence toward the validity and reliability of the results presented here.

Here, using MTMD studies we reported the interaction studies of P-gp substrate and inhibitor during the P-gp efflux cycle. The reported study gives an incisive understanding of the P-gp substrate and inhibitor molecular interactions. No distinct site for substrate and inhibitor binding was noticed, however, substantial difference in substrate and inhibitor binding interaction was noticed during the simulation from IO to OO state. The results clearly showed how substrate binding in the active site of P-gp gradually gets destabilized as the structure transform from IO to OO state. The results also showed a clear distinction between substrate and inhibitor interactions during P-gp catalytic cycle. The substrates loose their stable binding interactions and dislocate from actual binding site as the conformation of drug-binding residues gradually changed from IO to OO state, whereas the inhibitors maintained stable interactions with drug-binding residues, posing possibility of inhibition of the conformational change in P-gp structure. The residues F303, I306, F343, F728, I868, F942, T945 and A985 were found crucial for inhibitor interactions. The inhibitors in docking and MTMD experiments showed stable binding interactions with at least one of these residues depending on the binding site they occupied.

Apart from mechanistic insights drawn from MTMD simulations here, further MD simulation experiments would be required to reconcile in silico studies with experimental studies. For instance, the study here considered lowest energy docked pose in MTMD studies, however a ligand could bind in multiple orientations. It has been reported that

two substrates could bind simultaneous in drug-binding pocket and occupy different regions in the common drug-binding pocket [74]. Another set of simulation needs to be carried out to study how binding of two substrates will affect the movements and conformational changes in TM helices. Further, the MTMD technique could not be efficiently utilized to study the difference between substrate and inhibitor induced conformational changes in NBDs [75]. There are also biochemical evidences that the binding of nucleotide at NBDs induces conformational changes in TMDs [76]. Very long atomistic simulations would be further required to accommodate in silico experiments with these biochemical evidences.

The mechanistic picture of translocation of P-gp presented here, using MTMD studies gave sufficient details into conformational changes in drug-binding region, role of ICHs and topological arrangements of TM helices in P-gp translocation, and quantitative shifts TM helices providing valuable information for future experiments.

Abbreviations

P-gp	P-glycoprotein
TMD	trans-membrane domain
NBD	nucleotide binding domain
ICH	intracellular coupling helix
MTMD	multi-targeted molecular dynamics
IFD	induced fit docking
TM	trans-membrane.

Supplementary data to this article can be found online at http://dx.doi.org/10.1016/j.bbamem.2014.07.018.

Acknowledgement

The authors are thankful to the Department of Biotechnology (DBT), New Delhi (Grant number is BT/PR/14979/BID/07/353/2010), for financial support.

References

[1] R.L. Juliano, V. Ling, A surface glycoprotein modulating drug permeability in Chinese hamster ovary cell mutants, Biochim. Biophys. Acta 455 (1976) 152–162.
[2] H.S.L. Chan, G. Haddad, P.S. Thorner, G. DeBoer, Y.P. Lin, N. Ondrusek, H. Yeger, V. Ling, P-glycoprotein expression as a predictor of the outcome of therapy for neuroblastoma, N. Engl. J. Med. 325 (1991) 1608–1614.
[3] P.D.W. Eckford, F.J. Sharom, ABC efflux pump-based resistance to chemotherapy drugs, Chem. Rev. 109 (2009) 2989–3011.
[4] M.M. Gottesman, I. Pastan, The multidrug transporter, a double-edged sword, J. Biol. Chem. 263 (1988) 12163–12166.
[5] M. Hennessy, J.P. Spiers, A primer on the mechanics of P-glycoprotein the multidrug transporter, Pharmacol. Res. 55 (2007) 1–15.
[6] G. Szakács, J.K. Paterson, J.A. Ludwig, C. Booth-Genthe, M.M. Gottesman, Targeting multidrug resistance in cancer, Nat. Rev. Drug Discovery 5 (2006) 219–234.
[7] C.F. Higgins, R. Callaghan, K.J. Linton, M.F. Rosenberg, R.C. Ford, Structure of the multidrug resistance P-glycoprotein, Semin. Cancer Biol. 8 (1997) 135–142.
[8] P.M. Jones, A.M. George, Subunit interactions in ABC transporters: towards a functional architecture, FEMS Microbiol. Lett. 179 (1999) 187–202.
[9] F.J. Sharom, The P-glycoprotein efflux pump: how does it transport drugs? J. Membr. Biol. 160 (1997) 161–175.
[10] C.A. Shintre, A.C.W. Pike, Q. Li, J.-I. Kim, A.J. Barr, S. Goubin, L. Shrestha, J. Yang, G. Berridge, J. Ross, P.J. Stansfeld, M.S.P. Sansom, A.M. Edwards, C. Bountra, B.D. Marsden, F. von Delft, A.N. Bullock, O. Gileadi, N.A. Burgess-Brown, E.P. Carpenter, Structures of ABCB10, a human ATP-binding cassette transporter in apo- and nucleotide-bound states, Proc. Natl. Acad. Sci. U. S. A. 110 (2013) 9710–9715.
[11] R.J.P. Dawson, K.P. Locher, Structure of a bacterial multidrug ABC transporter, Nature 443 (2006) 180–185.
[12] A. Ward, C.L. Reyes, J. Yu, C.B. Roth, G. Chang, Flexibility in the ABC transporter MsbA: alternating access with a twist, Proc. Natl. Acad. Sci. U. S. A. 104 (2007) 19005–19010.
[13] S.G. Aller, J. Yu, A. Ward, Y. Weng, S. Chittaboina, R. Zhuo, P.M. Harrell, Y.T. Trinh, Q. Zhang, I.L. Urbatsch, G. Chang, Structure of P-glycoprotein reveals a molecular basis for poly-specific drug binding, Science 323 (2009) 1718–1722.
[14] M.S. Jin, M.L. Oldham, Q. Zhang, J. Chen, Crystal structure of the multidrug transporter P-glycoprotein from *Caenorhabditis elegans*, Nature 490 (2012) 566–569.
[15] J. Li, K.F. Jaimes, S.G. Aller, Refined structures of mouse P-glycoprotein, Protein Sci. (23) (2014) 34–46.
[16] J.D. Campbell, S.S. Deol, F.M. Ashcroft, I.D. Kerr, M.S.P. Sansom, Nucleotide-dependent conformational changes in HisP: molecular dynamics simulations of an ABC transporter nucleotide-binding domain, Biophys. J. 87 (2004) 3703–3715.
[17] J.D. Campbell, M.S.P. Sansom, Nucleotide binding to the homodimeric MJ0796 protein: a computational study of a prokaryotic ABC transporter NBD dimer, FEBS Lett. 579 (2005) 4193–4199.
[18] J.M. Damas, A.S.F. Oliveira, A.M. Baptista, C.M. Soares, Structural consequences of ATP hydrolysis on the ABC transporter NBD dimer: molecular dynamics studies of HlyB, Protein Sci. 20 (2011) 1220–1230.
[19] P.M. Jones, A.M. George, Mechanism of ABC transporters: a molecular dynamics simulation of a well characterized nucleotide-binding subunit, Proc. Natl. Acad. Sci. U. S. A. 99 (2002) 12639–12644.
[20] P.M. Jones, A.M. George, The ABC transporter structure and mechanism: perspectives on recent research, Cell. Mol. Life Sci. 61 (2004) 682–699.
[21] P.M. Jones, A.M. George, Nucleotide-dependent allostery within the ABC transporter ATP-binding cassette, J. Biol. Chem. 282 (2007) 22793–22803.
[22] P.M. Jones, A.M. George, Opening of the ADP-bound active site in the ABC transporter ATPase dimer: evidence for a constant contact, alternating sites model for the catalytic cycle, Proteins Struct. Funct. Genet. 75 (2009) 387–396.
[23] P.M. Jones, A.M. George, Molecular-dynamics simulations of the ATP/apo state of a multidrug ATP-binding cassette transporter provide a structural and mechanistic basis for the asymmetric occluded state, Biophys. J. 100 (2011) 3025–3034.
[24] A.S.F. Oliveira, A.M. Baptista, C.M. Soares, Insights into the molecular mechanism of an ABC transporter: conformational changes in the NBD dimer of MJ0796, J. Phys. Chem. B 114 (2010) 5486–5496.
[25] E.O. Oloo, E.Y. Fung, D.P. Tieleman, The dynamics of the MgATP-driven closure of MalK, the energy-transducing subunit of the maltose ABC transporter, J. Biol. Chem. 281 (2006) 28397–28407.
[26] P.C. Wen, E. Tajkhorshid, Dimer opening of the nucleotide binding domains of ABC transporters after ATP hydrolysis, Biophys. J. 95 (2008) 5100–5110.
[27] J.P. Becker, G. Depret, F. Van Bambeke, P.M. Tulkens, M. Pravost, Molecular models of human P-glycoprotein in two different catalytic states, BMC Struct. Biol. 9 (2009) 3.
[28] A. Ivetac, J.D. Campbell, M.S.P. Sansom, Dynamics and function in a bacterial ABC transporter: simulation studies of the BtuCDF system and its components, Biochemistry 46 (2007) 2767–2778.
[29] C. Kandt, D.P. Tieleman, Holo-BtuF stabilizes the open conformation of the vitamin B12 ABC transporter BtuCD, Proteins Struct. Funct. Genet. 78 (2010) 738–753.
[30] A.S. Oliveira, A.M. Baptista, C.M. Soares, Conformational changes induced by ATP-hydrolysis in an ABC transporter: a molecular dynamics study of the Sav 1866 exporter, Proteins Struct. Funct. Genet. 79 (2011) 1977–1990.
[31] E.O. Oloo, D.P. Tieleman, Conformational transitions induced by the binding of MgATP to the vitamin B12 ATP-binding cassette (ABC) transporter BtuCD, J. Biol. Chem. 279 (2004) 45013–45019.
[32] J. Sonne, C. Kandt, G.H. Peters, F.Y. Hansen, M.Ã. Jensen, D.P. Tieleman, Simulation of the coupling between nucleotide binding and transmembrane domains in the ATP binding cassette transporter BtuCD, Biophys. J. 92 (2007) 2727–2734.
[33] J.F. St-Pierre, A. Bunker, T. Rog, M. Karttunen, N. Mousseau, Molecular dynamics simulations of the bacterial ABC transporter SAV1866 in the closed form, J. Phys. Chem. B 116 (2012) 2934–2942.
[34] T.G. Sun, M. Liu, W.Z. Chen, C.X. Wang, Molecular dynamics simulation of the transmembrane subunit of BtuCD in the lipid bilayer, Sci. China Life Sci. 53 (2010) 620–630.
[35] P.C. Wen, E. Tajkhorshid, Conformational coupling of the nucleotide-binding and the transmembrane domains in ABC transporters, Biophys. J. 101 (2011) 680–690.
[36] J.W. Weng, K.N. Fan, W.N. Wang, The conformational transition pathway of ATP binding cassette transporter MsbA revealed by atomistic simulations, J. Biol. Chem. 285 (2010) 3053.
[37] M.L. O'Mara, A.E. Mark, The effect of environment on the structure of a membrane protein: P-glycoprotein under physiological conditions, J. Chem. Theory Comput. 8 (2012) 3964–3976.
[38] R.J. Ferreira, M.-J.U. Ferreira, D.J.V.A. dos Santos, Insights on P-glycoprotein's efflux mechanism obtained by molecular dynamics simulations, J. Chem. Theory Comput. 8 (2012) 1853–1864.
[39] R. Prajapati, U. Singh, A. Patil, K.S. Khomane, P. Bagul, A.K. Bansal, A.T. Sangamwar, In silico model for P-glycoprotein substrate prediction: insights from molecular dynamics and in vitro studies, J. Comput. Aided Mol. Des 27 (2013) 347–363.
[40] Schrödinger Suite 2009 Induced Fit Docking protocol; Glide version 5.5, Prime version 2.1, Schrödinger, LLC, New York, NY, 2009.
[41] W. Sherman, H.S. Beard, R. Farid, Use of an induced fit receptor structure in virtual screening, Chem. Biol. Drug Des. 67 (2006) 83–84.
[42] T.W. Loo, M.C. Bartlett, D.M. Clarke, Transmembrane segment 1 of human P-glycoprotein contributes to the drug-binding pocket, Biochem. J. 396 (2006) 537–545.
[43] T.W. Loo, M.C. Bartlett, D.M. Clarke, Transmembrane segment 7 of human P-glycoprotein forms part of the drug-binding pocket, Biochem. J. 399 (2006) 351–359.
[44] T.W. Loo, D.M. Clarke, Identification of residues in the drug-binding site of human P-glycoprotein using a thiol-reactive substrate, J. Biol. Chem. 272 (1997) 31945–31948.
[45] T.W. Loo, D.M. Clarke, Identification of residues within the drug-binding domain of the human multidrug resistance P-glycoprotein by cysteine-scanning mutagenesis and reaction with dibromobimane, J. Biol. Chem. 275 (2000) 39272–39278.
[46] T.W. Loo, M.C. Bartlett, D.M. Clarke, Disulfide cross-linking analysis shows that transmembrane segments 5 and 8 of human P-glycoprotein are close together on the cytoplasmic side of the membrane, J. Biol. Chem. 279 (2004) 7692–7697.
[47] T.W. Loo, M.C. Bartlett, D.M. Clarke, Val133 and Cys137 in transmembrane segment 2 are close to Arg935 and Gly939 in transmembrane segment 11 of human P-glycoprotein, J. Biol. Chem. 279 (2004) 18232–18238.

[48] T.W. Loo, M.C. Bartlett, D.M. Clarke, ATP hydrolysis promotes interactions between the extracellular ends of transmembrane segments 1 and 11 of human multidrug resistance P-glycoprotein, Biochemistry 44 (2005) 10250–10258.
[49] T.W. Loo, M.C. Bartlett, D.M. Clarke, Identification of residues in the drug translocation pathway of the human multidrug resistance P-glycoprotein by arginine mutagenesis, J. Biol. Chem. 284 (2009) 24074–24087.
[50] T.W. Loo, M.C. Bartlett, D.M. Clarke, Human P-glycoprotein contains a greasy ball-and-socket joint at the second transmission interface, J. Biol. Chem. 288 (2013) 20326–20333.
[51] T.W. Loo, D.M. Clarke, Drug-stimulated ATPase activity of human P-glycoprotein requires movement between transmembrane segments 6 and 12, J. Biol. Chem. 272 (1997) 20986–20989.
[52] T.W. Loo, D.M. Clarke, Identification of residues in the drug-binding domain of human P-glycoprotein. Analysis of transmembrane segment 11 by cysteine-scanning mutagenesis and inhibition by dibromobimane, J. Biol. Chem. 274 (1999) 35388–35392.
[53] T.W. Loo, D.M. Clarke, The packing of the transmembrane segments of human multidrug resistance P-glycoprotein is revealed by disulfide cross-linking analysis, J. Biol. Chem. 275 (2000) 5253–5256.
[54] T.W. Loo, D.M. Clarke, Determining the dimensions of the drug-binding domain of human P-glycoprotein using thiol cross-linking compounds as molecular rulers, J. Biol. Chem. 276 (2001) 36877–36880.
[55] T.W. Loo, D.M. Clarke, Defining the drug-binding site in the human multidrug resistance P-glycoprotein using a methanethiosulfonate analog of verapamil MTS-verapamil, J. Biol. Chem. 276 (2001) 14972–14979.
[56] T.W. Loo, D.M. Clarke, Cross-linking of human multidrug resistance P-glycoprotein by the substrate, tris-(2-maleimidoethyl) amine, is altered by ATP hydrolysis evidence for rotation of a transmembrane helix, J. Biol. Chem. 276 (2001) 31800–31805.
[57] T.W. Loo, D.M. Clarke, Drug rescue distinguishes between different structural models of human P-glycoprotein, Biochemistry 52 (2013) 7167–7169.
[58] T.W. Loo, D.M. Clarke, A salt bridge in intracellular loop 2 is essential for folding of human P-glycoprotein, Biochemistry 52 (2013) 3194–3196.
[59] X. Zhang, K.I. Collins, L.M. Greenberger, Functional evidence that transmembrane 12 and the loop between transmembrane 11 and 12 form part of the drug-binding domain in P-glycoprotein encoded by MDR1, J. Biol. Chem. 270 (1995) 5441–5448.
[60] I.L. Urbatsch, B. Sankaran, S. Bhagat, A.E. Senior, Both P-glycoprotein nucleotide-binding sites are catalytically active, J. Biol. Chem. 270 (1995) 26956–26961.
[61] M.L. Oldham, J. Chen, Snapshots of the maltose transporter during ATP hydrolysis, Proc. Natl. Acad. Sci. U. S. A. 108 (2011) 15152–15156.
[62] J.G. Wise, Catalytic transitions in the human MDR1 P-glycoprotein drug-binding sites, Biochemistry 51 (2012) 5125–5141.
[63] T.W. Loo, D.M. Clarke, Location of the rhodamine-binding site in the human multidrug resistance P-glycoprotein, J. Biol. Chem. 277 (2002) 44332–44338.
[64] S. Dey, M. Ramachandra, I. Pastan, M.M. Gottesman, S.V. Ambudkar, Evidence for two nonidentical drug-interaction sites in the human P-glycoprotein, Proc. Natl. Acad. Sci. U. S. A. 94 (1997) 10594–10599.
[65] C. Pascaud, M. Garrigos, S. Orlowski, Multidrug resistance transporter P-glycoprotein has distinct but interacting binding sites for cytotoxic drugs and reversing agents, Biochem. J. 333 (1998) 351–358.
[66] A.B. Shapiro, K. Fox, P. Lam, V. Ling, Stimulation of P-glycoprotein-mediated drug transport by prazosin and progesterone, Eur. J. Biochem. 259 (1999) 841–850.
[67] M.R. Lugo, F.J. Sharom, Interaction of LDS-751 with P-glycoprotein and mapping of the location of the R drug-binding site, Biochemistry 44 (2005) 643–655.
[68] T.W. Loo, M.C. Bartlett, D.M. Clarke, Permanent activation of the human P-glycoprotein by covalent modification of a residue in the drug-binding site, J. Biol. Chem. 278 (2003) 20449–20452.
[69] T.W. Loo, D.M. Clarke, Identification of the distance between the homologous halves of P-glycoprotein that triggers the high/low ATPase activity switch, J. Biol. Chem. 289 (2014) 8484–8492.
[70] T.W. Loo, D.M. Clarke, Functional consequences of phenylalanine mutations in the predicted transmembrane domain of P-glycoprotein, J. Biol. Chem. 268 (1993) 19965–19972.
[71] I.K. Pajeva, C. Globisch, M. Wiese, Structure–function relationships of multidrug resistance P-glycoprotein, J. Med. Chem. 47 (2004) 2523–2533.
[72] T.W. Loo, M.C. Bartlett, D.M. Clarke, Substrate-induced conformational changes in the transmembrane segments of human P-glycoprotein. Direct evidence for the substrate-induced fit mechanism for drug binding, J. Biol. Chem. 278 (2003) 13603–13606.
[73] T.W. Loo, D.M. Clarke, Locking intracellular helices 2 and 3 together inactivates human P-glycoprotein, J. Biol. Chem. 289 (2014) 229–236.
[74] T.W. Loo, M.C. Bartlett, D.M. Clarke, Simultaneous binding of two different drugs in the binding pocket of the human multidrug resistance P-glycoprotein, J. Biol. Chem. 278 (2003) 39706–39710.
[75] T.W. Loo, M.C. Bartlett, D.M. Clarke, Drug binding in human P-glycoprotein causes conformational changes in both nucleotide-binding domains, J. Biol. Chem. 278 (2003) 1575–1578.
[76] T.W. Loo, M.C. Bartlett, D.M. Clarke, Nucleotide binding, ATP hydrolysis, and mutation of the catalytic carboxylates of human P-glycoprotein cause distinct conformational changes in the transmembrane segments, Biochemistry 46 (2007) 9328–9336.